

# Lacustrine diatom oxygen isotopes as palaeo precipitation proxy - Holocene environmental and snowmelt variations recorded at Lake Bolshoye Shchuchye, Polar Urals, Russia

Hanno Meyer<sup>1</sup>, Svetlana Kostrova<sup>1</sup>, Philip Meister<sup>1</sup>, Marlene M. Lenz<sup>2</sup>, Gerhard Kuhn<sup>3</sup>, Larisa Nazarova<sup>1</sup>, Liudmila Syrykh<sup>4</sup>, and Yuri Dvornikov<sup>5</sup>

<sup>1</sup>Alfred Wegener Institute Helmholtz Centre for Polar and Marine Research

<sup>2</sup>University of Cologne

<sup>3</sup>Alfred-Wegener-Institut Helmholtz-Zentrum für Polar- und Meeresforschung

<sup>4</sup>Herzen State Pedagogical University of Russia

<sup>5</sup>Department of Landscape Design and Sustainable Ecosystem

November 22, 2022

## Abstract

The diatom oxygen isotope composition ( $\delta^{18}\text{O}_{\text{diatom}}$ ) from lacustrine sediments helps tracing the hydrological and climate dynamics in individual lake catchments, and is generally linked to changes in temperature and  $\delta^{18}\text{O}_{\text{lake}}$ . Lake Bolshoye Shchuchye (67°53'N; 66°19' E; 186 m a.s.l) is the largest and deepest freshwater reservoir in the Polar Urals, Arctic Russia. Its  $\delta^{18}\text{O}_{\text{diatom}}$  record generally follows a decrease in summer insolation and the northern hemisphere (NH) temperature history. However, it displays exceptional, short-term variations exceeding 5centennial-scale variability occurs contemporaneously with and similarly to Holocene NH glacier advances. However, larger Holocene glacier advances in the Lake Bolshoye Shchuchye catchment are unknown and have not left any significant imprint on the lake sediment record. As Lake Bolshoye Shchuchye is deep and voluminous, about 30-50% of its volume needs to be exchanged with isotopically different water within decades to account for these shifts in the  $\delta^{18}\text{O}_{\text{diatom}}$  record. A plausible source of water with light isotope composition inflow is snow, known to be transported in surplus by snow redistribution from the windward to the leeward side of the Polar Urals. Here, we propose snow melt and influx changes being the dominant mechanism responsible for the observed short-term changes in the  $\delta^{18}\text{O}_{\text{diatom}}$  record. This is the first time such drastic, centennial-scale hydrological changes in a catchment have been identified in Holocene lacustrine diatom oxygen isotopes, which, for Lake Bolshoye Shchuchye, are interpreted as proxy for summer temperatures and palaeo precipitation.

1 **Lacustrine diatom oxygen isotopes as palaeo precipitation proxy - Holocene**  
2 **environmental and snowmelt variations recorded at Lake Bolshoye**  
3 **Shchuchye, Polar Urals, Russia**

4  
5 **Hanno Meyer<sup>1</sup>, Svetlana S. Kostrova<sup>1</sup>, Philip Meister<sup>1</sup>, Marlene M. Lenz<sup>2</sup>, Gerhard Kuhn<sup>3</sup>,**  
6 **Larisa Nazarova<sup>1,4</sup>, Liudmila S. Syrykh<sup>5</sup>, Yury Dvornikov<sup>6</sup>.**

7  
8 <sup>1</sup> Alfred Wegener Institute Helmholtz Centre for Polar and Marine Research, Research Unit  
9 Potsdam, Telegrafenberg A45, Potsdam 14473, Germany

10 <sup>2</sup> Institute of Geology and Mineralogy, University of Cologne, Zùlpicher Str. 49a, Cologne  
11 50674, Germany

12 <sup>3</sup> Alfred Wegener Institute Helmholtz Centre for Polar and Marine Research, Am Alten Hafèn  
13 26, Bremerhaven 27568, Germany

14 <sup>4</sup> Kazan Federal University, Kremlyovskaya str. 18, Kazan 420018, Russia

15 <sup>5</sup> Herzen State Pedagogical University of Russia, Moika 48, St. Petersburg 191186, Russia

16 <sup>6</sup> Department of Landscape Design and Sustainable Ecosystems, Agrarian-Technological  
17 Institute, Peoples' Friendship University of Russia (RUDN University), 6 Miklukho-Maklaya St,  
18 Moscow, 117198, Russia.

19  
20 Corresponding author: Hanno Meyer ([hanno.meyer@awi.de](mailto:hanno.meyer@awi.de)). ORCID: 0000-0003-4129-4706

21  
22 **Key Points:**

- 23 • Diatom oxygen isotopes from sediments of Lake Bolshoye Shchuchye are valuable  
24 proxies for the Holocene hydrological and climate dynamics
- 25 • Centennial-scale variability of the Holocene diatom isotope record is contemporaneous to  
26 glacier advances in the Northern hemisphere
- 27 • Snow melt variability in the lake catchment is the main driver for the short-term changes  
28 in  $\delta^{18}\text{O}_{\text{diatom}}$

29

30       **Abstract**

31       The diatom oxygen isotope composition ( $\delta^{18}\text{O}_{\text{diatom}}$ ) from lacustrine sediments helps tracing  
32 the hydrological and climate dynamics in individual lake catchments, and is generally linked to  
33 changes in temperature and  $\delta^{18}\text{O}_{\text{lake}}$ . Lake Bolshoye Shchuchye (67°53'N; 66°19' E; 186 m a.s.l.)  
34 is the largest and deepest freshwater reservoir in the Polar Urals, Arctic Russia. Its  $\delta^{18}\text{O}_{\text{diatom}}$   
35 record generally follows a decrease in summer insolation and the northern hemisphere (NH)  
36 temperature history. However, it displays exceptional, short-term variations exceeding 5%,  
37 especially in Mid and Late Holocene. This centennial-scale variability occurs  
38 contemporaneously with and similarly to Holocene NH glacier advances. However, larger  
39 Holocene glacier advances in the Lake Bolshoye Shchuchye catchment are unknown and have  
40 not left any significant imprint on the lake sediment record. As Lake Bolshoye Shchuchye is  
41 deep and voluminous, about 30–50% of its volume needs to be exchanged with isotopically  
42 different water within decades to account for these shifts in the  $\delta^{18}\text{O}_{\text{diatom}}$  record. A plausible  
43 source of water with light isotope composition inflow is snow, known to be transported in  
44 surplus by snow redistribution from the windward to the leeward side of the Polar Urals. Here,  
45 we propose snow melt and influx changes being the dominant mechanism responsible for the  
46 observed short-term changes in the  $\delta^{18}\text{O}_{\text{diatom}}$  record. This is the first time such drastic,  
47 centennial-scale hydrological changes in a catchment have been identified in Holocene lacustrine  
48 diatom oxygen isotopes, which, for Lake Bolshoye Shchuchye, are interpreted as proxy for  
49 summer temperatures and palaeo precipitation.

50

51       **Keywords**

52       stable oxygen isotopes, hydrological fluctuations, biogenic silica, diatoms, climate change,  
53 chironomids, lake sediments

54

55

56

## 57 **1. Introduction**

58 The ongoing climate warming is currently being debated at scientific, political and social  
59 levels. Comparisons with past climatic conditions are generally used to assess the stability or  
60 instability of regional environments as well as the potential to predict possible trends of future  
61 climate change. This is important for policymakers today and for human well-being in the future  
62 as food and water supply, energy production and use largely depend on the successful  
63 reconstructions of climatic conditions that existed in the past (IPCC, 2014; NOAA NCEI, 2020).

64 Glaciers and ice or snow fields are visual indicators for climate changes in high mountain  
65 regions (Davis et al., 2009; Khromova et al., 2014, 2019; Solomina et al., 2015; WGMS, 2017).  
66 Their advances and retreats do not only significantly alter landscapes (Khromova et al., 2019),  
67 but can also increase risks of local hazards and natural disasters (Huggel et al., 2008; Petrakov et  
68 al., 2008; Khromova et al., 2019). Changes in glacier mass balances lead to rearrangements of  
69 local and regional water cycles (Koboltschnig & Schöner, 2011; Radić & Hock, 2014; Nazarova  
70 et al., 2021a) and may be linked to global sea level rise (Shahgedanova et al., 2012; Gardner et  
71 al., 2013).

72 The Ural Mountains are a north-to-south stretching range of more than 2,000 km, separating  
73 Europe and Asia. As such, it is an orographic barrier playing an important role for atmospheric  
74 moisture transport to the Eurasian Arctic (i.e. Svendsen et al., 2004). In this region, small  
75 glaciers are widespread, mainly in the Polar Urals (Kononov et al., 2005; Shahgedanova et al.,  
76 2012; Khromova et al., 2014; Solomina et al., 2015; Svendsen et al., 2019). Field-based and  
77 satellite observations revealed that significant changes in air temperature and precipitation in  
78 recent decades have caused a reduction of the glacier areas in the Polar Urals by 23% on average  
79 (Nosenko & Tsvetkov, 2003; Shahgedanova et al., 2012; Khromova et al., 2014; 2019).  
80 Although numerous studies have contributed to a better understanding of the climate and  
81 environmental history in the Polar Urals (Panova et al., 2003; Cremer et al., 2004; Andreev et al.,

82 2005; Jankovská et al., 2006; Solovieva et al., 2008; Regnéll et al., 2019; Nazarova et al.,  
83 2021b), the glacier fluctuations in this region are still very poorly investigated (Kononov et al.,  
84 2005; Solomina et al., 2010, 2015; Haflidason et al., 2019) and existing knowledge of the glacier  
85 dynamics history remains fragmentary (Mangerud et al., 2008; Astakhov, 2018; Svendsen et al.,  
86 2014, 2019). Thus, reliable proxy data are required to reconstruct the long-term glacial history of  
87 the region in more detail.

88 Continuous reconstructions of glacier size variations are based on information provided by  
89 different parameters from lake sediments, e.g. magnetic susceptibility, loss-on-ignition, grain-  
90 size variations, and chemical element contents (Dahl et al., 2003; Nesje, 2009; Nesje et al., 2014;  
91 Regnéll et al., 2019; Lenz et al., 2021). The oxygen isotope composition of diatoms ( $\delta^{18}\text{O}_{\text{diatom}}$ )  
92 has been widely used as a proxy for climate and hydrological changes in many studies (Swann  
93 and Leng, 2009; van Hardenbroek et al., 2018). Shifts in diatom oxygen isotope records  
94 (Kostrova et al., 2013, 2019, 2021; Meyer et al., 2015; Cartier et al., 2019), often reflect changes  
95 in lake water ( $\delta^{18}\text{O}_{\text{lake}}$ ) related to variations in atmospheric precipitation patterns and/or in the  
96 hydrological conditions (evaporation, meltwater supply) in the catchment.  $\delta^{18}\text{O}_{\text{diatom}}$ ,  
97 consequently, has a high potential to enhance our understanding of coupled glacier-lake  
98 dynamics beyond the instrumental records.

99 In the current study,  $\delta^{18}\text{O}_{\text{diatom}}$  from Lake Bolshoye Shchuchye (Fig. 1) has been employed as  
100 novel proxy to trace environmental and climatic fluctuations in the Polar Urals through the  
101 Holocene. Our approach is supported by lake-internal proxies (i.e. chironomid and  
102 biogeochemical analyses) of the same sedimentary succession, complemented by modern isotope  
103 hydrology and isotope mass-balance modeling. The newly obtained  $\delta^{18}\text{O}_{\text{diatom}}$  record is discussed  
104 in the context of other regional and hemispheric environmental reconstructions (Andreev et al.,  
105 2005; Jankovská et al., 2006; Regnéll et al., 2019; Svendsen et al., 2019; Lenz et al., 2021;  
106 Cowling et al., 2021) including glacier fluctuations in order to explore the response of the lake  
107 system to hydroclimate change.

108

109

## 110 **2. Study area**

111 Lake Bolshoye Shchuchye (67°53'N; 66°19' E; 186 m a.s.l) is the largest and deepest  
112 freshwater reservoir of the Polar Urals, Arctic Russia, located in the permafrost zone at the  
113 boundary between Europe and Asia (Fig. 1). The lake surface area is 11.8 km<sup>2</sup>, with mean and  
114 maximum water depths of 78.2 m and 160.0 m, respectively (Pechkin et al., 2017). The lake  
115 basin consists of a tectonic, glacially-eroded and overdeepened V-shaped mountain valley  
116 (Kemmerich, 1966; Svendsen et al., 2019; Haflidason et al., 2019) orientated northwest to  
117 southeast (Fig. 1B). With an average width of 0.92 km (maximum of 1.35 km) and a length of  
118 12.7 km (Bogdanov et al., 2004), the lake is clearly elongated in shape. The lake is surrounded  
119 by ridges which peak up to more than 1000 m (Kemmerich, 1966). The lake basin is  
120 characterized by steep slopes and a sharp increase in depth in the central part and more gentle  
121 slopes in the northwestern and southeastern parts (Kemmerich, 1966; Pechkin et al., 2017). The  
122 bedrock comprises Proterozoic-Cambrian basaltic and andesitic rocks in the eastern and  
123 northwestern parts of the catchment and Ordovician quartzite and phyllitic rocks in the  
124 southwestern catchment (Dushin et al., 2009; Lammers et al., 2019; Svendsen et al., 2019). The  
125 catchment area of ~227 km<sup>2</sup> consists of a narrow zone along the lake as well as a wider  
126 hinterland to the north (Bogdanov et al., 2004). The lake is a hydrologically open system fed by  
127 12 ephemeral streams with Pyryanatanë River as the main inflow forming a delta at the lake's  
128 northern end (Bogdanov et al., 2004). The Bolshaya Shchuchya River outflows at the southern  
129 part of the lake (Fig. 1B). The annual runoff from the catchment area is around 0.13–0.15 km<sup>3</sup>  
130 a<sup>-1</sup> and about 5–7 years of residence time are required to renew the whole volume of water (~1  
131 km<sup>3</sup>) stored in the lake basin (Haflidason et al., 2019).

132 Lake Bolshoye Shchuchye is monomictic with mixing occurring only during the very short  
133 summer periods (Svendsen et al., 2019). The lake water temperature is persistently low, reaching

134 1.2–3.1°C beneath the ice (Regnéll et al., 2019) and a mean surface water temperature not  
135 exceeding 10–14 °C even on very hot days in August (Mitrofanova, 2017; Vinokurova, 2017).  
136 The lake is typically ice-covered for more than half a year, from early October to ice-out in late  
137 June–early July (Kemmerich, 1966; Svendsen et al., 2019). The lake ecosystem is pristine, and  
138 not subject to anthropogenic impact and changes only under the influence of natural factors  
139 (Yermolaeva & Burmistrova, 2017).

140 The regional climate is continental and quite severe with long, cold winters and short, cool  
141 summers. The catchment is characterized by excessive moisture with a lack of heat (Morozova et  
142 al., 2006). The average annual air temperature is –6.3 °C (at the Bolshaya Khadata station (260  
143 m a.s.l) located ~25 km to the south of Lake Bolshoye Shchuchye; Fig. 1A), ranging from –14.3  
144 °C (winter) to +7.0 °C (summer) (Solomina et al., 2010). Annual precipitation amounts are  
145 around 610 mm with the sum of warm period precipitation of 70 mm on average (Solomina et  
146 al., 2010; Shahgedanova et al., 2012). There are a few cirque- and niche-type glaciers less than 1  
147 km<sup>2</sup> in size near the lake catchment today (Solomina et al., 2010; Khromova et al., 2014; Regnéll  
148 et al., 2019). However, glaciers almost disappeared in response to the recent climate warming  
149 (Svendsen et al., 2019).

150 The hydroclimate in this region reflects the trajectories of prevailing air masses. Typically,  
151 westerly cyclones originating over the Northern Atlantic dominate in winter, bringing cloudy,  
152 windy weather and precipitation (Kemmerich, 1966; Kononov et al., 2005; Shahgedanova et al.,  
153 2012; Pischalnikova, 2016). These are also related to strong winds that cause snow redistribution  
154 within mountains and its accumulation on leeward slopes and depressions (Mangerud et al.,  
155 2008). In summer, dry continental air masses from the east provide conditions for relatively hot  
156 and dry weather, whereas incursions of northwesterly and northerly cyclones often cause rain  
157 and a sharp drop in air temperatures (Kemmerich, 1966; Kononov et al., 2005).

158

### 159 **3. Materials and methods**

### 3.1. Sediment recovery, core lithology and chronology

In April 2016, a 54-m-long sediment core (Co 1321; 67°53' N, 66°19' E; water depth: 136 m) was retrieved from the central part of Lake Bolshoye Shchuchye using gravity and percussion piston corers (UWITEC Ltd., Austria) from the central part of Lake Bolshoye Shchuchye (Fig. 1). The depth interval from 9.15 to 0 mcd (meter composite depth) of the core, consisting of grey to brown fine-grained, diffusely layered, hemipelagic sediment intermitted by turbidite layers, is the focus of this paper. A recent study (Lenz et al., 2021) demonstrated that the upper 9.15-m part was deposited during the last ~11,400 years (calendar ages are used consistently in this study), i.e. covers the Holocene interglacial. The age-depth relationship of the analysed part of the Co1321 core is based on the surface age (AD 2016) and five AMS <sup>14</sup>C dates. The age model was calculated with CLAM version 2.3.9 (Blaauw, 2010, 2021), which was run in R version 4.0.3 (R core Team, 2020). The Holocene onset at ~ 11.5 cal. ka BP is supported by the results of pollen analysis. A detailed description of the age model and lake internal parameters of Lake Bolshoye Shchuchye are given in Lenz et al. (2021).

### 3.2. Geochemical analyses

The Co 1321 core was X-ray fluorescence (XRF)-scanned at 1-mm resolution using an ITRAX core scanner (Cox Analytical, Sweden) at the University of Cologne. Sub-sampling for total carbon (TC) and total inorganic carbon (TIC) analyses was done in 8-cm intervals omitting turbidites, which offers a temporal resolution of about 100 years between two samples. TC and TIC contents were measured with a DIMATOC 2000 carbon analyser (Dimatec Corp., Germany). Total organic carbon (TOC) was calculated by subtracting TIC from TC (Lenz et al., 2021).

### 3.3. Biogenic silica analysis, diatom preparation and contamination assessment

185 Biogenic silica (BSi) analysis was performed on 0.45 g of dry sediment sampled from Co  
186 1321. Samples were ground and analysed for BSi using the automated sequential leaching  
187 method (Müller & Schneider, 1993) at the Alfred Wegener Institute Helmholtz Centre for Polar  
188 and Marine Research (AWI Bremerhaven, Germany). Biogenic opal was calculated from BSi  
189 assuming a 10% water content within the frustule (Mortlock & Froelich, 1989; Müller &  
190 Schneider, 1993).

191 A total of 48 Holocene sediment samples with an initial biogenic opal content (Fig. 2) above  
192 8% were processed for  $\delta^{18}\text{O}_{\text{diatom}}$  analysis. Diatom purification involved a multi-step procedure  
193 based on Chaplignin et al. (2012a). First, sediment samples were heated to 50 °C in 35%  $\text{H}_2\text{O}_2$  for  
194 three days to remove organic matter, before adding 10% HCl to eliminate carbonates. To  
195 separate diatoms from the detrital contaminants with higher density, samples were centrifuged in  
196 sodium polytungstate (SPT;  $3\text{Na}_2\text{WO}_4 \cdot 9\text{WO}_3 \cdot \text{H}_2\text{O}$ ) heavy liquid solution (at decreasing densities  
197 from 2.50 to 2.10  $\text{g cm}^{-3}$ ) at 2500 rpm for 30 minutes. The detritus was retained for a  
198 contamination assessment and  $\delta^{18}\text{O}_{\text{diatom}}$  correction. Hardly soluble micro-organic and lighter  
199 contaminants were removed by applying an inverse separation with SPT of 2.05  $\text{g cm}^{-3}$ . Purified  
200 diatoms were then washed in ultra-pure water using a 3  $\mu\text{m}$  filter. Finally, samples were wet  
201 sieved using a Rhewum Schallfix nylon mesh and sonication system, resulting in two diatom size  
202 fractions (3–10  $\mu\text{m}$  and >10  $\mu\text{m}$ ). Only the 3–10  $\mu\text{m}$  fraction yielded sufficient material (>2 mg)  
203 to be used for  $\delta^{18}\text{O}_{\text{diatom}}$  analysis.

204 Energy-Dispersive X-ray Spectroscopy (EDS) under a scanning electron microscope (SEM)  
205 at the German Research Centre for Geosciences (GFZ Potsdam, Germany) was used to assess  
206 contamination of all diatom samples (Chaplignin et al., 2012a). The EDS data (Table 1; Fig. 2)  
207 indicate that all 48 purified samples contained sufficient diatom material and less than 2.5%  
208  $\text{Al}_2\text{O}_3$  (Chaplignin et al., 2012a) to be analysed for  $\delta^{18}\text{O}_{\text{diatom}}$ . 32 samples were highly purified,  
209 comprising between 97.1 and 98.8%  $\text{SiO}_2$ , and 0.5–1.6%  $\text{Al}_2\text{O}_3$ , respectively. 16 samples were  
210 less pure with 94.8–96.8%  $\text{SiO}_2$ , and 1.3–2.0%  $\text{Al}_2\text{O}_3$ .

211

### 212 3.4. Diatom isotope analysis and $\delta^{18}\text{O}_{\text{diatom}}$ correction

213 The oxygen isotope composition of purified diatom samples ( $n = 48$ ) and the detrital  
214 contaminant sub-samples ( $n = 5$ ) were measured at the ISOLAB Facility at AWI Potsdam with a  
215 PDZ Europa 2020 mass spectrometer. Prior to isotope analysis, exchangeable oxygen was  
216 removed using inert Gas Flow Dehydration (iGFD) under Argon gas at  $1100\text{ }^{\circ}\text{C}$ , after Chaplignin  
217 et al. (2010). Dehydrated samples were fully reacted using laser fluorination with  $\text{BrF}_5$  as reagent  
218 to liberate  $\text{O}_2$  (Clayton & Mayeda, 1963) and then directly measured against an oxygen reference  
219 sample of known isotopic composition. Replicate analyses of the calibrated working standard  
220 BFC (Chaplignin et al., 2011) yielded  $\delta^{18}\text{O} = +28.82 \pm 0.26\text{‰}$  ( $n=76$ ) indicating an accuracy and  
221 analytical precision corresponding to the method's long-term analytical reproducibility ( $1\sigma$ ) of  
222  $\pm 0.25\text{‰}$  (Chaplignin et al., 2010).

223 All measured diatom  $\delta^{18}\text{O}$  values were contamination-corrected using the geochemical mass-  
224 balance approach (Swann & Leng, 2009; Chaplignin et al., 2012a):

$$225 \quad \delta^{18}\text{O}_{\text{corr}} = \left( \delta^{18}\text{O}_{\text{meas}} - \frac{\delta^{18}\text{O}_{\text{cont}} \cdot c_{\text{cont}}}{100} \right) / \left( \frac{c_{\text{diatom}}}{100} \right) \quad (1)$$

226 where  $\delta^{18}\text{O}_{\text{meas}}$  is the original measured  $\delta^{18}\text{O}$  value of the sample.  $\delta^{18}\text{O}_{\text{corr}}$  is the measured  $\delta^{18}\text{O}$   
227 value corrected for contamination, with  $\delta^{18}\text{O}_{\text{cont}} = +12.8 \pm 0.6\text{‰}$  ( $n = 5$ ), which represents the  
228 average  $\delta^{18}\text{O}$  of the heavy detrital fractions after the first heavy liquid separation. The  
229 percentages of contamination ( $c_{\text{cont}}$ ) and diatom material ( $c_{\text{diatom}}$ ) within the analyzed sample are  
230 calculated using the EDS-measured  $\text{Al}_2\text{O}_3$  content of the individual sample divided by the  
231 average  $\text{Al}_2\text{O}_3$  content of the contamination ( $21.5 \pm 1.0\%$  in heavy fractions,  $n = 5$ ) and as  $(100\% -$   
232  $c_{\text{cont}})$ , respectively.

233

### 234 3.5. Water sampling and stable water isotope analysis

235 During the drilling campaign, lake water samples were collected in a depth profile of the  
236 water column between the lake ice cover and bottom ( $n = 17$ ), at the same location as the

237 sediment core (Fig. 1B). Additionally, a 2.0-m snow profile was sampled from the surface of the  
238 snowpack to ground level in 10–15 cm intervals ( $n = 20$ ). Snow samples were melted at room  
239 temperature. All water samples were stored cool in airtight bottles prior to stable isotope  
240 analyses.

241 Hydrogen ( $\delta D$ ) and oxygen ( $\delta^{18}O$ ) stable water isotopes were analyzed at the AWI ISOLAB  
242 Facility, Potsdam, Germany with a Finnigan MAT Delta-S mass spectrometer using equilibration  
243 techniques with an analytical uncertainty ( $1\sigma$ ) of better than  $\pm 0.8\%$  for  $\delta D$  and  $\pm 0.1\%$  for  $\delta^{18}O$   
244 (Meyer et al., 2000). The secondary parameter deuterium excess is calculated as  $d = \delta D - 8 \cdot$   
245  $\delta^{18}O$  (Dansgaard, 1964). Data are given as per mil difference (‰) to V-SMOW and compared to  
246 the Global Meteoric Water Line (GMWL; Craig, 1961) and to the Local Meteoric Water Line  
247 (LMWL) based on Global Network for Isotopes in Precipitation data of Salekhard (GNIP;  
248 IAEA/WMO, 2021) as the nearest station.

249

### 250 3.6. Isotopic mass-balance modeling

251 Isotopic mass-balance modeling was performed simulating varying amount and isotopic  
252 composition of surface inflow as well as evaporative enrichment on Lake Bolshoye Shchuchye.  
253 The goal of this was to determine both the potential impact of these factors on lake water  
254 isotopic composition and the speed of the reaction.

255 Assuming constant lake volume and hydrological parameters, the lake water isotopic  
256 composition after a given time can be calculated according to Gonfiantini (1986):

$$257 \quad \delta^{18}O_{lake} = \delta^{18}O_S - (\delta^{18}O_S + \delta^{18}O_0) * e^{-(1+mx) * \left(\frac{t}{V}\right)} \quad (2)$$

258 where  $\delta^{18}O_0$  is the initial isotopic composition of lake water and  $\delta^{18}O_S$  the steady-state  
259 composition approached over time. The latter can be expressed as:

$$260 \quad \delta^{18}O_S = \frac{\delta^{18}O_I + mx\delta^{18}O^*}{1+mx} \quad (3)$$

261 The limiting isotope enrichment  $\delta^{18}O^*$  is calculated according to Gat (1981),  $m$  and  $x$   
262 represent the temporal enrichment slope and the fraction of lake water lost by evaporation,

263 respectively. For further elaboration on this approach, we refer to Darling et al. (2006) and  
264 references therein. The inflow isotopic composition  $\delta^{18}\text{O}_I$  was assumed to be equal to  $\delta^{18}\text{O}_0$  and  
265 to  $\delta^{18}\text{O}$  of mean annual precipitation (-17.8‰). Mean annual precipitation and mean summer  
266 precipitation were modeled using the Online Isotopes in Precipitation Calculator (OIPC; Bowen,  
267 2021), c.f. chapter 4.2. Since data for evaporation are not readily available, the amount of  
268 evaporation from the lake surface was approximated as a function of summer mean air  
269 temperature  $T$ , atmospheric humidity  $h$ , altitude  $a$  and latitude  $A$  (Linacre, 1977).

$$270 \quad E_0 = \frac{700 \frac{T_m}{100-A} + 15(T - T_d)}{(80 - T)} \left( \frac{\text{mm}}{d} \right) \quad (4)$$

271 where  $T_m = T + 0.006a$  and the dew-point  $T_d$  is approximated according to Lawrence (2005) as  
272  $T_d \approx T - \left( \frac{1-h}{5} \right)$ . Assuming an ice-free period of 100 days per year, the calculated daily  
273 evaporation rates were multiplied by 100 to obtain annual values. The isotopic composition of  
274 atmospheric moisture was calculated according to Gibson et al. (1999) based on summer  
275 precipitation.

276

### 277 3.7. Chironomid analysis

278 Eighty-four samples were prepared for chironomid analysis with standard techniques  
279 (Brooks et al., 2007). Chironomid identification followed Wiederholm (1983) and Brooks et al.  
280 (2007).

281 The ratio of lotic (moving water or riverine) and lentic (standing water) chironomid taxa in  
282 sediments of the Lake Bolshoye Shchuchye, and chironomid-inferred mean July air temperature  
283 ( $T_{\text{air}}$ ) are in the focus of this study. In this context, increasing representation of the lotic fauna  
284 reflects stronger runoff and more intensive water input with the inflowing rivers (Nazarova et al.,  
285 2017c; Biskaborn et al., 2019). For information on ecology of chironomid taxa, we refer to  
286 Brooks et al. (2007), Stief et al. (2005), Moller Pilot (2009, 2013), and Nazarova et al. (2011,  
287 2015, 2017a, b). The reconstruction of mean July air temperatures was performed using the

288 North Russian (NR) chironomid-based temperature inference model (WA-PLS, 2 component;  $r^2$   
289 boot = 0.81; RMSEP boot=1.43 °C) (Nazarova et al., 2015).

290

### 291 3.8. Digital elevation model preparation and delineation of the lake catchment

292 The freely distributed digital elevation model (DEM) ArcticDEM (Porter et al., 2018) was  
293 used for Lake Bolshoye Shchuchye catchment delineation and morphometric analysis of the  
294 catchment. Raw 10-m resolution ArcticDEM data covering the area of interest were downloaded  
295 from the Polar Geospatial Center data portal (<https://www.pgc.umn.edu/data/arcticdem/>).  
296 Contours at 20-m intervals were extracted from the DEM and were manually corrected for  
297 artefacts and missing patches in order to build up a hydrologically correct digital terrain model  
298 (DTM). This improved DTM was created by interpolating corrected contours using the  
299 TopoToRaster algorithm with drainage enforcement (Hutchinson, 1989) within the ESRI©  
300 ArcGIS 10.2 software. The catchment of Lake Bolshoye Shchuchye was extracted based on the  
301 hydrologically correct topographic representation within QGIS 3.10 software. For morphometric  
302 analysis, topographic variables were obtained, including slopes, aspects, total curvature, flow  
303 direction, flow accumulation. All topographic variables were calculated with R (R Core Team,  
304 2017) using the packages ‘raster’ (Robert & van Etten, 2012), ‘dynatopmodel’ (Quinn et al.,  
305 1995) and ‘spatialEco’ (Evans, 2020).

306

### 307 3.9. Calculation of the snow water equivalent within the catchment

308 The catchment polygon was further used to analyze the distribution of snow depth and snow  
309 water equivalent (SWE). Snow depth within the lake catchment at 10-m resolution was  
310 calculated using auxiliary data: cumulative snow probability for snow melt period of 2019  
311 extracted from Sentinel-2 time series and snow depth ranges (0–845 cm of snow) measured  
312 within ten snow survey profiles within the neighboring lake Bol’shaya Khadata catchment  
313 (Gokhman & Zhidkov, 1979). The atmospherically corrected (sen2cor, ESA) Sentinel-2 Level-

314 2A data archive was analyzed in order to calculate the cumulative snow probability value for the  
315 entire catchment. Level-2A data provide the snow probability band scaled from 0 to 1 based on  
316 the specific spectral signature of snow cover, where values of 0 and 1 correspond to 0% snow  
317 and 100% snow, respectively. For the 2019 glaciological year (October–May; Ivanov, 2013), we  
318 obtained all images (less than 20% clouds) and filtered out all scenes covering less than 85% of  
319 the lake catchment without clouds. Further, all snow probability bands of these images were  
320 summarized to calculate a cumulative value: there were seven scenes meeting the requirements  
321 covering the period from May 8, 2019 (maximum of snow) to July 25, 2019 (quasi-complete  
322 melting of snow). Within the range of cumulative snow probability, the range of snow depth was  
323 scaled to measured snow depths of the neighboring catchment in 1978 (Gokhman & Zhidkov,  
324 1979). The SWE was calculated based on the empirical relationship between snow depth and  
325 SWE obtained for tundra landscape in Central Yamal (500 km to the North from the lake)  
326 according to Dvornikov et al. (2015). All satellite image analysis and calculations were  
327 performed within Google Earth Engine Cloud Computing platform (Gorelick et al., 2017).

328

## 329 **4. Results**

### 330 4.1. Stable water isotopes

331 The results of stable water isotope analyses are presented in a  $\delta^{18}\text{O}$ – $\delta\text{D}$  diagram (Fig. 3). One  
332 water sample taken directly at the ice-water boundary (Fig. 4A) and one surface snow sample  
333 (Fig. 4C) were excluded from interpretation due to significantly different isotopic signals from  
334 those for other samples; likely due to interaction between water phases. The average recent water  
335 isotope composition of Lake Bolshoye Shchuchye is  $-15.9\pm 0.2\text{‰}$  for  $\delta^{18}\text{O}_{\text{lake}}$ ,  $-114.4\pm 2.6\text{‰}$  for  
336  $\delta\text{D}_{\text{lake}}$  and  $+13.0\pm 0.5\text{‰}$  for  $d$  excess ( $n = 16$ ). The water column  $\delta^{18}\text{O}$ -profile reveals no  
337 substantial changes with depth (Fig. 4A). Small variations of  $0.5\text{‰}$  were detected at 10 m depth,  
338 incoherent with  $T_{\text{lake}}$  changes (Fig. 4B). A positive ( $0.08 \text{‰}/\text{°C}$ ), but statistically not significant  
339 ( $R^2 = 0.14$ ) correlation was found between  $\delta^{18}\text{O}_{\text{lake}}$  and  $T_{\text{lake}}$ .

340 The snow cover displays a large variability between single layers in their  $\delta^{18}\text{O}_{\text{snow}}$  and  $\delta\text{D}_{\text{snow}}$   
341 values ranging from  $-25.1$  to  $-15.2\text{‰}$  and from  $-190.1$  to  $-103.1\text{‰}$ , respectively. The  $d$  excess  
342 ranges from  $+2.7$  to  $+18.9\text{‰}$ . The minimum  $\delta^{18}\text{O}_{\text{snow}}$  with  $-25.1\text{‰}$  is reached at the depth of 115  
343 cm.  $\delta^{18}\text{O}_{\text{snow}}$  values demonstrate a continuous decrease of  $\sim 0.07\text{‰}/\text{cm}$  in the lower (195–115  
344 cm) part of the column (Fig. 4C). Visible variations in  $\delta^{18}\text{O}_{\text{snow}}$  with smaller maxima at depths of  
345 10, 75 and 105 cm occur in the upper section (115–0 cm) of the core. In general, this interval  
346 displays a gradual increase of  $\sim 0.09\text{‰}\cdot\text{cm}^{-1}$  in  $\delta^{18}\text{O}_{\text{snow}}$  values.

347 As precipitation samples could not be collected at Lake Bolshoye Shchuchye, mean annual  
348  $\delta^{18}\text{O}_{\text{prec}}$  and  $\delta\text{D}_{\text{prec}}$  values of regional precipitation have been derived from the GNIP database  
349 (IAEA/WMO, 2021) for Salekhard (16 m a.s.l) situated  $\sim 150$  km southeast of the lake (Fig. 1A).  
350 Additionally,  $\delta^{18}\text{O}_{\text{prec}}$  and  $\delta\text{D}_{\text{prec}}$  values as well as a LMWL were modelled for the drilling  
351 location based on the algorithm published by Bowen and Revenaugh (2003) and Bowen et al.  
352 (2005) using the OIPC (Bowen, 2021). Modelled  $\delta^{18}\text{O}_{\text{prec}}$  and  $\delta\text{D}_{\text{prec}}$  values of  $-17.8\pm 0.4\text{‰}$  and  
353  $-135.0\pm 3.0\text{‰}$  (Bowen, 2021) are consistent with GNIP values of  $-17.5\pm 1.7\text{‰}$  and  
354  $-136.1\pm 13.2\text{‰}$ , respectively (IAEA/WMO, 2021). The LMWL based on modelled values was  
355 determined as:  $\delta\text{D} = 7.7 \delta^{18}\text{O} + 2.6\text{‰}$  ( $R^2 = 1.00$ ; Fig. 3; Bowen, 2021) and is in a good  
356 agreement with the LMWL from GNIP data (IAEA/WMO, 2021) with a slope of 7.9 and an  
357 intercept of  $+1.2\text{‰}$  ( $R^2 = 0.99$ ; Fig. 3). Minor offsets between the LMWLs are mainly due to  
358 differences in both temporal and spatial domains. Due to the distance of Salekhard to the  
359 sampling location, we assume the modelled  $\delta^{18}\text{O}_{\text{prec}}$  and  $\delta\text{D}_{\text{prec}}$  values and the LMWL to be more  
360 reliable for Lake Bolshoye Shchuchye.

361

## 362 4.2 Oxygen isotope record

363 The Lake Bolshoye Shchuchye diatom  $\delta^{18}\text{O}_{\text{corr}}$  values (further referred to as  $\delta^{18}\text{O}_{\text{diatom}}$ ) range  
364 from  $+23.4\text{‰}$  to  $+31.8\text{‰}$  (Fig. 4; Table 1) and exhibit the same trend as  $\delta^{18}\text{O}_{\text{meas}}$  values.  
365 Contamination correction leads to an offset of  $\delta^{18}\text{O}_{\text{corr}}$  towards higher values of about  $0.7\text{‰}$  in

366 the upper part of the core (younger than 8.5 cal. ka BP) and 1.3‰ higher for the lower part (older  
367 than 8.5 cal. ka BP).

368 The Co 1321 core is characterized by a mean  $\delta^{18}\text{O}_{\text{diatom}}$  value of +27.0‰ for the complete  
369 Holocene. In Early Holocene (11.4 to 7 cal. ka BP), the  $\delta^{18}\text{O}_{\text{diatom}}$  values are with +27.3±0.8‰  
370 slightly higher than the Holocene mean. Highest mean  $\delta^{18}\text{O}_{\text{diatom}}$  values with +27.9±2.0‰ are  
371 observed in Mid Holocene (7 to 5 cal. ka BP), whereas lowest  $\delta^{18}\text{O}_{\text{diatom}}$  values of +26.3±1.7‰  
372 characterize the Late Holocene (5 cal. ka BP to present). The maximum  $\delta^{18}\text{O}_{\text{diatom}}$  value  
373 (+31.8‰) in the record is registered at 6.3 cal. ka BP. The absolute minimum in the  $\delta^{18}\text{O}_{\text{diatom}}$   
374 record occurs at the sediment surface at 0.0 cal. ka BP with +23.7‰. Sharp variations are  
375 observed every ~0.7–1.5 cal. ka with smaller maxima at 1.0, 1.9, 2.6, 3.7, 4.6, 6.4, 7.1, 8.1, 9.2,  
376 10.1 and 10.5 cal. ka BP and smaller minima at 1.7, 2.4, 3.0, 4.1, 5.8, 6.6, 7.3, 8.3, 10.4 and 10.9  
377 cal. ka BP. In general, a gradual depletion of ~0.39‰/1000 years is visible between 10.9 and 0.0  
378 cal. ka BP (Fig. 4).

379

#### 380 4.3 Chironomids

381 The chironomid fauna of Lake Bolshoye Shchuchye is dominated by cold-tolerant lentic taxa  
382 usual for Arctic lakes. Several taxa characteristic for lotic environments have been found in the  
383 lake sediments. Among them are taxa from the subfamilies Diamesinae (e.g. *Diamesa aberrata*-  
384 type, *D. cinerella*-type, *D. bertrami*-type), that usually inhabit small, cold running streams and  
385 brooks and Orthocladiinae (e.g. *Eukiefferiella*, *Metriocnemus*, *Thienemanniella clavicornis*-type,  
386 *Tvetenia bavarica*-type), that occur in flowing waters and surf zones of the lakes.

387 Representation of the lotic taxa varies considerably reaching 50% of the fauna during the  
388 Early Holocene (at ~10.6 cal. ka BP) (Fig. 4). However, rather high concentration of lotic  
389 chironomids (25–33% of the fauna) have been observed between 7.7 and 4.5 cal. ka BP.  
390 Between 4.5 and 3.2 cal. ka BP, no lotic taxa appear in the lake, indicating a decrease of the  
391 water inflow (Fig. 4). At 3.2 cal. ka BP, lotic chironomids appear in the lake again and their

392 abundance reaches 25% of the fauna. Between 3.2 and 0 cal. ka BP, the abundance of lotic taxa  
393 remains at 11% in average, and it rises to 31% towards the modern times.

394 The chironomid-based reconstructed  $T_{\text{air}}$  during the Early Holocene are in average  $\sim 1.5$  °C  
395 below modern level. The transition to the Mid Holocene is characterized by an increase in  
396 chironomid abundancies with a gradual rise in the reconstructed  $T_{\text{air}}$  to the modern level (10.6  
397 °C). Between  $\sim 8.0$  and 3.2 cal. ka BP, the  $T_{\text{air}}$  are the highest and reach up to 3 °C above the  
398 present  $T_{\text{air}}$  at 5.5 cal. ka BP. However, there is a cooling tendency in  $T_{\text{air}}$  after 5.5 cal. ka BP,  
399 when reconstructed  $T_{\text{air}}$  gradually decrease and reach  $\sim 1$  °C below the modern  $T_{\text{air}}$  at  $\sim 1.7$  cal. ka  
400 BP. Chironomid-based reconstructed  $T_{\text{air}}$  are slightly above modern values between 1.0 to 0.6 cal  
401 ka BP, subsequently decreasing to the present level.

402

## 403 5. Discussion

### 404 5.1. Isotope hydrology

405 When interpreting lacustrine  $\delta^{18}\text{O}_{\text{diatom}}$  records, a proper understanding of the modern  
406 hydrology is a precondition for assessing possible past hydrological changes.

407 The recent mean Bolshoye Shchuchye  $\delta^{18}\text{O}_{\text{lake}}$  of  $-15.8\text{‰}$  is slightly higher than the regional  
408  $\delta^{18}\text{O}_{\text{prec}}$  of  $-17.8\text{‰}$  (Bowen, 2021). Additionally, the lake water isotope samples plot on the  
409 GMWL and slightly above the modelled LMWL (Fig. 3) and follow a linear dependency with a  
410 slope of 7.2 and an intercept of +0.3 ( $R^2 = 0.90$ ;  $n = 16$ ). This suggests that  $\delta^{18}\text{O}_{\text{lake}}$  roughly  
411 corresponds to  $\delta^{18}\text{O}_{\text{prec}}$ , slightly shifted to more positive values probably due to seasonality  
412 effects.

413 At the same time, water samples are situated close to the GMWL (Fig. 3), indicating the  
414 absence of major evaporation effects in recent times. The V-shape of the lake basin, almost  
415 completely surrounded by steep slopes, allows for lake level fluctuations without significant  
416 changes in the lake surface area and water volume.

417 Palaeogeographical and geomorphological studies yielded pre-Holocene Bolshoye  
418 Shchuchye lake level fluctuations with a highstand 8 m above present lake level along parts of  
419 the western shore (Svendsen et al., 2019). This higher than modern lake level might have  
420 resulted from intense meltwater influx from contemporaneous glaciers in the lake catchment and  
421 a simultaneous damming of the lake by a glacifluvial fan at the south outlet until around 14–15  
422 cal. ka BP (Svendsen et al., 2019). The lake level dropped when this fan was incised by glacial  
423 meltwaters (Regnéll et al., 2019). Additionally, seismic profiles point to lower lake levels prior  
424 to 15 cal. ka BP (Haflidason et al., 2019). A terrace in the northern part of Lake Bolshoye  
425 Shchuchye documents a 2–3 m higher lake level at ~2–3 cal. ka BP (Svendsen et al., 2019).  
426 Therefore, lake level changes and associated evaporation effects cannot be fully excluded at  
427 Lake Bolshoye Shchuchye, especially during the Last Glacial Maximum and the early  
428 deglaciation period, but are assumed to be weak for the Holocene, the period of interest.

429 The water  $\delta^{18}\text{O}_{\text{lake}}$  depth profile shows a constant isotope composition (Fig. 4A) and suggests  
430 a well-mixed water column lacking any isotopic stratification, at least in spring 2016. There is no  
431 notable relationship between  $\delta^{18}\text{O}_{\text{lake}}$  and  $T_{\text{lake}}$  (Fig. 4A, B). Hence, water column temperature  
432 effects are assumed to be of minor importance on  $\delta^{18}\text{O}_{\text{lake}}$ .

433 The snow cover isotope samples plot on or close to the GMWL (Fig. 3) in the co-isotope  
434 diagram with a slope of 7.9 and an intercept of +10.8 ( $R^2 = 0.96$ ). The mean  $\delta^{18}\text{O}_{\text{snow}}$  of  $-20.4\text{‰}$   
435 ( $d$  excess =  $+12.9\text{‰}$ ) is slightly higher than the regional mean  $\delta^{18}\text{O}_{\text{prec}}$  of  $-22.8\text{‰}$  ( $d$  excess =  
436  $+8.4\text{‰}$ ) between October and April (when precipitation fall as snow) derived from the OIPC  
437 (Bowen, 2021). This likely represents a seasonal bias towards late winter and spring snow, but  
438 could also include effects of sublimation, evaporation and wind drift processes altering the snow  
439 pack's isotopic composition over time (Friedman et al., 1991; Nikolaev & Mikhalev, 1995). The  
440  $\delta^{18}\text{O}_{\text{snow}}$  profile displays variations with depth (Fig. 4C) which might be associated with isotopic  
441 differences between individual precipitation (or deposition) events persisting despite snow  
442 metamorphism (Friedman et al., 1991). Nevertheless, as  $T_{\text{air}}$  is a primary control of  $\delta^{18}\text{O}_{\text{prec}}$

443 especially in polar regions (Dansgaard, 1964), it is likely that the isotopically lightest layers  
444 (110–130 cm) with  $\delta^{18}\text{O}_{\text{snow}}$  of  $-24$  to  $-25\text{‰}$  were formed during the coldest months  
445 (January–February). Generally, it can be concluded that snow can be a source of isotopically-  
446 depleted water draining into the lake.

447 In summary, Lake Bolshoye Shchuchye is a well-mixed, non-evaporative and isotopically  
448 rather uniform lake, which is mainly fed by meteoric waters, i. e. precipitation with an important  
449 contribution of melting snow from higher altitudes. Although there are indications of evaporation  
450 effects in the past, we suggest the precipitation signal ( $\delta^{18}\text{O}_{\text{prec}}$ ) to be most relevant for  $\delta^{18}\text{O}_{\text{lake}}$ .

451

## 452 5.2. Isotope fractionation and main controls on $\delta^{18}\text{O}_{\text{diatom}}$

453 Variations in  $\delta^{18}\text{O}_{\text{diatom}}$  values of lacustrine sediment are mainly controlled by changes in  
454 water temperature ( $T_{\text{lake}}$ ) and/or the corresponding  $\delta^{18}\text{O}_{\text{lake}}$  (Labeyrie, 1974; Juillet-Leclerc &  
455 Labeyrie, 1987; Leng & Barker, 2006; Dodd & Sharp, 2010).

456 When comparing the overall Holocene average Lake Bolshoye Shchuchye  $\delta^{18}\text{O}_{\text{diatom}}$  of  
457  $+27.0\text{‰}$  with the recent average  $\delta^{18}\text{O}_{\text{lake}}$  of  $-15.9\text{‰}$ , a fractionation coefficient  $\alpha_{(\text{silica-water})} =$   
458  $(1000 + \delta^{18}\text{O}_{\text{diatom}})/(1000 + \delta^{18}\text{O}_{\text{lake}})$  (Juillet-Leclerc & Labeyrie, 1987) of 1.0436 was  
459 determined. This yields an isotopic enrichment  $\Delta^{18}\text{O}_{\text{SiO}_2\text{-H}_2\text{O}} = 42.9\text{‰}$  corresponding to a  $T_{\text{lake}}$   
460 of  $4.5\text{ °C}$  that matches well the blooming temperature of the diatom species *Aulacoseira*  
461 *subarctica* ( $\sim 4\text{ °C}$ ; Gibson et al., 2003; Lepskaya et al., 2010) dominant in the sediments of the  
462 lake (A. Ludikova, pers. comm.). This suggests that the  $\delta^{18}\text{O}_{\text{diatom}}$  values at Lake Bolshoye  
463 Shchuchye (Table 1), are the right order of magnitude and, consequently, underline the general  
464 applicability of the diatom isotope signal for palaeoreconstructions at the lake.

465 To test whether temperature effects are the dominant forcing responsible for the short-term  
466 variability in  $\delta^{18}\text{O}_{\text{diatom}}$  of up to  $5\text{‰}$ , we calculated a scenario function displaying possible  
467 changes in  $T_{\text{air}}$  and  $T_{\text{lake}}$ . We used the aforementioned  $\delta^{18}\text{O}_{\text{diatom}}$ -temperature coefficient of  
468  $-0.2\text{‰}/\text{°C}$  (Dodd & Sharp, 2010) and the regional temperature relation between monthly mean

469  $\delta^{18}\text{O}_{\text{prec}}$  and  $T_{\text{air}}$  of  $\delta^{18}\text{O}_{\text{prec}} = +0.34\text{‰}/\text{°C}$  (Salekhard; IAEA/WMO, 2021). The scenario function  
470 for a 5‰-shift as visible in the Bolshoye Shchuchye diatom isotope record constitutes a linear  
471 function, the slope of which is defined by the quotient of the  $T_{\text{lake}}$  and  $T_{\text{air}}$  coefficients (Figure  
472 S1). Intercept and Zero of the function represent "traditional" interpretations of temperature  
473 effects regarding either  $T_{\text{lake}}$  or  $T_{\text{air}}$  alone, respectively. The former suggests a drop in  $T_{\text{lake}}$  of  
474 25°C while the latter corresponds to a rise in  $T_{\text{air}}$  of 14.7°C needed to explain the shifts of 5‰ in  
475  $\delta^{18}\text{O}_{\text{diatom}}$ . Due to the fact that present lake temperature changes in the course of an annual cycle  
476 amount to 7–11 °C only (Mitrofanova, 2017; Vinokurova, 2017; Regnéll et al., 2019), variations  
477 of 25°C during the summer period (diatom bloom) are highly unlikely. Consequently,  $T_{\text{lake}}$  alone  
478 cannot be the primary control and rather plays a subordinate role in explaining  $\delta^{18}\text{O}_{\text{diatom}}$  in Lake  
479 Bolshoye Shchuchye. Similarly, a 14.7°C increase in  $T_{\text{air}}$  is unlikely and contrasts with only ~3-4  
480 °C from pollen reconstructions (Andreev et al., 2005) and maximum 6°C from the current  
481 chironomid-based reconstruction for the complete Holocene (Fig. 4). Other mathematically  
482 possible combinations of  $T_{\text{air}}$  and  $T_{\text{lake}}$  (points plotting on the scenario function) are not plausible  
483 either as they would require even more pronounced changes of  $T_{\text{air}}$  and  $T_{\text{lake}}$ .

484 Since Lake Bolshoye Shchuchye currently does not show evaporative enrichment, we  
485 conclude the isotopic composition of the inflow to be main driver of the lake water isotopic  
486 composition and, hence, of the  $\delta^{18}\text{O}_{\text{diatom}}$  record. Inflow, in turn, largely reflects precipitation, but  
487 with temperature effects ruled out as the single decisive factor, such changes can only be  
488 attributed to atmospheric circulation changes or hydrological processes within the lake's  
489 catchment.

490 Reorganization of the atmospheric transport patterns in Early Holocene after the decay of the  
491 Eurasian Ice Sheet around ~10 cal. ka BP, allowed moisture from the North Atlantic to enter the  
492 region, in line with the northward migration of the treeline. Forest conditions persisted in the  
493 catchment until ~4 cal. ka BP, when the treeline retreated back south (Clarke et al., 2020).  
494 Today, westerly/northwesterly cyclones originating over the Atlantic (the Northern and

495 Norwegian seas) moving across Scandinavia to the Taymyr Peninsula bring relatively warm and  
496 moist air masses to the Polar Urals year-round, especially in winter (Kononov et al., 2005;  
497 Shahgedanova et al., 2012; Pischalnikova, 2016). Relatively cold northerly cyclones forming  
498 around the Novaya Zemlya archipelago over the Barents and Kara seas deliver comparably less  
499 moisture (Kononov et al., 2005; Morozova et al., 2006). However, this northerly influence might  
500 have increased over the Holocene with a reduced sea ice concentration in the Kara and Barents  
501 Sea sectors. Moreover, recycled moisture from regional terrestrial surface waters might  
502 contribute through evaporation/evapotranspiration in summer (Bonne et al., 2020) in line with  
503 the establishment of forests in the catchment. Changes in the relative contribution of these  
504 moisture sources to the local water balance can therefore shift  $\delta^{18}\text{O}_{\text{lake}}$  and  $\delta^{18}\text{O}_{\text{diatom}}$  both  
505 towards higher and lower  $\delta^{18}\text{O}$  values, but relative changes should be visible in regional  
506 palaeoenvironmental reconstructions. In summary, the changes in the Lake Bolshoye Shchuchye  
507  $\delta^{18}\text{O}_{\text{diatom}}$ , are mainly driven by changes in  $\delta^{18}\text{O}_{\text{lake}}$  signal, affected by  $T_{\text{air}}$ , atmospheric  
508 circulation and local hydrological conditions.

509

### 510 5.3. The Bolshoye Shchuchye $\delta^{18}\text{O}_{\text{diatom}}$ record

511 The diatom isotope record displays higher overall values of  $+27.4\pm 1.3\text{‰}$  in Early- to Mid-  
512 Holocene (with the absolute maximum  $\delta^{18}\text{O}_{\text{diatom}}$  of  $+31.8\text{‰}$  at 6.4 cal. ka BP) and lower values  
513 of  $+26.4\pm 1.7\text{‰}$  in Mid- to Late Holocene (with a clear minimum of  $+23.2\text{‰}$  at the surface  
514 corresponding to the most recent, ~100 years old sediments). Generally, a gradual decrease in  
515  $\delta^{18}\text{O}_{\text{diatom}}$  of ~3–4‰ over the Holocene is notable in the Bolshoye Shchuchye  $\delta^{18}\text{O}_{\text{diatom}}$  record,  
516 especially when considering the minima (Fig. 4). This is in line with the summer insolation  
517 decrease at 60°N (Berger & Loutre, 1991). Insolation reaches a maximum in Early Holocene and  
518 a minimum in Late Holocene, i.e. during the Little Ice Age (LIA). The high overall variability in  
519 the Bolshoye Shchuchye  $\delta^{18}\text{O}_{\text{diatom}}$  record ( $\Delta^{18}\text{O}$  of 8.6‰) results from both this trend with

520 higher  $\delta^{18}\text{O}_{\text{diatom}}$  values in the first half of the Holocene and lower values in the Late Holocene as  
521 well as short-term fluctuations superimposed upon this trend.

522 These fluctuations consist of short term (centennial-scale) maxima and minima of more than  
523 5‰, setting the Bolshoye Shchuchye  $\delta^{18}\text{O}_{\text{diatom}}$  record apart from most other diatom isotope  
524 records stemming from high-latitude open lakes. Since these variations in  $\delta^{18}\text{O}_{\text{diatom}}$  are in most  
525 cases based on more than one data point they are unlikely to be artefacts related to sample  
526 preparation or contamination correction issues.

527 The key questions are (1) which processes may be responsible for these short-term variations  
528 in  $\delta^{18}\text{O}_{\text{diatom}}$  and (2) whether these processes are related to a larger scale pattern, visible in other  
529 lake-internal proxies and beyond or rather singular observations for Lake Bolshoye Shchuchye.

530 Generally, high-latitude lacustrine diatom isotope records from open lakes are rather smooth  
531 depending on depth, volume and residence time of the lake under consideration (Swann et al.,  
532 2010; Chaplgin et al., 2012b; Kostrova et al., 2019, 2021). These records vary usually by 3–5‰  
533 over the entire Holocene and have been interpreted taking into account the individual  
534 hydrological situation and isotopic background of each lake. As a consequence, short-term  
535 fluctuations seldomly exceed 2‰ and have been found (but not interpreted) as single-point  
536 spikes in Lake Kotokel, a very shallow, highly evaporative lake (Kostrova et al., 2013, 2014).  
537 Moreover, two short-term negative excursions of 4–5‰ have been described in a published  
538  $\delta^{18}\text{O}_{\text{diatom}}$  record only, at 4.7 and 1.4 cal. ka BP for Lake Chuna on Kola Peninsula (Jones et al.  
539 2004).

540 Isotopic mass-balance modeling (Fig. 5) shows the potential impact of evaporative  
541 enrichment on Lake Bolshoye Shchuchye for three different scenarios, ranging from present  
542 conditions to hypothetic much lower annual precipitation and atmospheric humidity. While  
543 evaporation can indeed impart an effect of ~2‰ within several decades, it fails to reproduce the  
544 magnitude of the short-term fluctuations observed in the Lake Bolshoye Shchuchye record.

545 The difference between present-day conditions (precipitation 610 mm/a,  $h=0.9$ ) and the most  
546 arid, hypothetical scenario (200 mm/a,  $h=0.7$ ) amounts to an isotopic enrichment of only 1.85‰.  
547 These results, in conjunction with the fact that Lake Bolshoye Shchuchye currently does not  
548 exhibit an evaporative signature, suggest that there must be a different locally-confined influence  
549 on the water isotope composition to explain the minima and maxima in the  $\delta^{18}\text{O}_{\text{diatom}}$  record.

550 Large-scale atmospheric patterns (i.e. shifts in the moisture transport and precipitation  
551 regime, seasonality of precipitation) seem unlikely as they would have an influence on a larger  
552 region that should be visible in other proxies and regional datasets as well and would lead to  
553 rather moderate changes. Changes in lake ice coverage, and hence, seasonality of the diatom  
554 bloom seem also unlikely processes as these would also change moderately in a deep basin as  
555 Lake Bolshoye Shchuchye.

556 For a significant change in the isotope composition of a lake, another option is substitution of  
557 lake water, i.e. a certain volume being replaced by isotopically different water. In mountainous  
558 areas such as the Polar Urals, water of lighter isotope composition than the lake itself might be  
559 glacier or snow melt waters draining from higher altitudes into the lake (i. e. Meyer et al., 2015).  
560 Taking into account the recent  $\delta^{18}\text{O}_{\text{lake}}$  of -15.8‰ and assuming the present-day volume as  
561 constant and 100%, it can be calculated, how much water needs to be exchanged in Lake  
562 Bolshoye Shchuchye to explain an isotopic difference  $\Delta^{18}\text{O}$  of 5‰. If this isotopically different  
563 inflow would correspond to the lightest snow measured within the catchment (-25‰; Fig. 3C),  
564 corresponding to a ~10‰ offset compared to  $\delta^{18}\text{O}_{\text{lake}}$ , about 55% of the lake water (equal to 0.55  
565  $\text{km}^3$ ) need to be exchanged. Assuming lower snow endmember values of -30‰ and -35‰, less  
566 water would need to be replaced, but still amounting to 35% and 26% of the lake volume,  
567 respectively.

568 Adding large amounts of water from a different than usual source (with different water  
569 isotope composition) or cutting off the major source for a certain period could, hence,  
570 substantially change the isotope composition of the lake. At Two-Jurts-Lake (Kamchatka), the

571 diatom isotope composition follows summer insolation, but changes in Neoglacial times due to  
572 the addition of isotopically light water from melting glaciers (Meyer et al., 2015) even though  
573 there is currently no glaciation in the catchment. The more glacial meltwaters reach the lake, the  
574 more negative the inflow  $\delta^{18}\text{O}$  and, hence,  $\delta^{18}\text{O}_{\text{lake}}$ . Less meltwater would imply lower  
575 contribution of isotopically light influx. If Lake Bolshoye Shchuchye received large amounts of  
576 meltwater, this should be notable both in the sediment and hydrological records.

577

#### 578 5.4. Glacier fluctuations

579 Glacier fluctuations are poorly constrained in the Russian Arctic, including the Polar Urals  
580 (Kononov et al., 2005; Solomina et al., 2010, 2015; Haflidason et al., 2019). It is known though  
581 that the glaciers in the Urals display exceptional changes in local accumulation (and ablation)  
582 budgets (Mangerud et al., 2008). Westerlies, especially in the winter season, favor accumulation  
583 of snow on leeward sides of the mountains. This process, combined with snow avalanches, leads  
584 to extremely high local accumulation rates, which may be several times higher than local  
585 precipitation (Mangerud et al., 2008). Therefore, the situation on leeward sides of the Ural  
586 Mountains allows for short-term changes of the local accumulation and water balance, and  
587 hence, implies the possibility of contribution of light isotopic (winter and/or high altitude)  
588 precipitation to the lake.

589 Svendsen et al. (2019) performed a detailed assessment of the glacial and environmental  
590 changes in the Polar Urals including geomorphological description, exposure ages and lake  
591 sediment coring. In their study, they concluded on a larger glaciation in the region during stage  
592 MIS 4, and more restricted mountain glaciers in MIS 2 and MIS 3, but only small glaciers in  
593 shaded areas of the Polar Urals during MIS 1 that formed during Late Holocene cooling. For the  
594 Ural Mountains, an endmoraine and glacier advances during the Little Ice Age (LIA) age have  
595 been described (Mangerud et al., 2008).

596 A possibility to test our hypothesis of glacial meltwaters triggering centennial-scale changes  
597 in  $\delta^{18}\text{O}_{\text{lake}}$  is a comparison with northern hemispheric (or Eurasian) glacial fluctuations as  
598 summarized in Solomina et al. (2015). Here, the Russian Arctic is poorly constrained, but several  
599 glacial advances have been described in Neoglacial times, generally associated with regional  
600 cooling i.e. for Franz Josef Land with a prominent advance in the LIA (Lubinsky et al., 1999).  
601 However, regional compilations of dated glacier advances exist for the Alps (Ivy-Ochs, 2009),  
602 Scandinavia (Nesje, 2009) or semi-arid Asia (Dortch et al., 2013), summarized in Solomina et al.  
603 (2015).

604 Especially striking is the similarity to the Scandinavian reconstruction (Nesje, 2009) with  
605 described glacial advances at 0.2–0.7, 1.6, 2.3, 3.3, 4.4, 5.6 cal. ka BP, corresponding to  
606 prominent minima in the Bolshoye Shchuchye  $\delta^{18}\text{O}_{\text{diatom}}$  record (Fig. 4), which would  
607 correspond to enhanced influx of glacial meltwaters, either due to more winter precipitation or  
608 meltwater entering the lake lowering  $\delta^{18}\text{O}_{\text{lake}}$ . Other prominent minima in the  $\delta^{18}\text{O}_{\text{diatom}}$  record at  
609 6.6–6.8 and 7.4–7.7 cal. ka BP are, however, not found in the Scandinavian reconstruction by  
610 Nesje (2009), but either in the Alps, in Norway (Matthews & Dresser, 2008) or in semi-arid Asia  
611 (Dortch et al., 2013).

612 The centennial-scale fluctuations in the  $\delta^{18}\text{O}_{\text{diatom}}$  record are contemporaneous with northern  
613 hemisphere glacier advances, described for other Eurasian regions. Therefore, maxima in the  
614 Bolshoye Shchuchye  $\delta^{18}\text{O}_{\text{diatom}}$  record could hence be associated with either reduced meltwater  
615 or winter precipitation influx to the lake either due to lower precipitation amounts or less snow  
616 transported to the leeward side of the Ural Mountains.

617 High-resolution glacier mass balance studies in the Polar Urals provide (additional) evidence  
618 for short-term snow changes in the region, with a generally positive glacier mass balance in the  
619 Little Ice Age (LIA) and a negative mass balance after 1850 (Kononov et al., 2005). LIA  
620 moraines have been described for several glaciers in the Polar Urals, including the Chernov and  
621 Obruchev glaciers (Mangerud et al., 2008). The second part of the 20th century shows a

622 pronounced tendency towards glacier shrinkage, with solid precipitation in the region being  
623 generally lower than the ablation (Khromova et al., 2014; 2019).

624

#### 625 5.5. Lake-internal parameters

626 In order to test whether the strong variability in the Holocene  $\delta^{18}\text{O}_{\text{diatom}}$  record at Lake  
627 Bolshoye Shchuchye with their clear, short-term centennial-scale fluctuations is also reflected in  
628 the lakes' sedimentary record, we inter-compare diatom isotopes and lake-internal parameters  
629 from Lenz et al. (2021). These parameters (Fig. 4) supposedly react on fast and major changes in  
630 the catchment hydrology and include abiotic (clay content and Ti cps) as well as biotic proxies  
631 (TOC, biogenic opal contents and chironomids).

632 All these proxies display some internal variability throughout the Holocene, but do not  
633 reveal statistically significant relationships with the  $\delta^{18}\text{O}_{\text{diatom}}$  record. During the Early  
634 Holocene the observed high representation of lotic chironomids can be related to a very poor  
635 lacustrine fauna at this time. Lotic chironomids are brought by riverine influx, i.e. fed by water  
636 from snowmelt and enrich the lake benthic communities. Decrease in the share of lotic taxa  
637 thereafter can be related to a better development of the lacustrine fauna under milder climatic  
638 conditions during the Mid Holocene. At ~7.5 to 8.5 cal. ka BP, when  $\delta^{18}\text{O}_{\text{diatom}}$  shows a  
639 maximum and the diatom isotope variability increases clearly, a major phase shift is obvious in  
640 all lake-internal proxies with absolute maxima in biogenic opal, TOC and chironomid-derived  
641 summer  $T_{\text{air}}$ , as well as absolute minima in Ti and clay values.

642 At 7.5 cal. ka BP, the lake-internal parameters show a slight decrease in biogenic opal and  
643 chironomid-based summer temperatures, a moderate increase in Ti cps, and rather constant  
644 values in clay and TOC contents. Biogenic opal as indicator of the lakes' diatom production and  
645 chironomid-derived  $T_{\text{July}}$  show similarities to the diatom isotope record such as common Mid  
646 Holocene maxima and Late Holocene minima. Meltwater events should lead to enhanced  
647 nutrient supply to the lake and, thus, a higher biogenic opal concentration in the core. Some

648 minima, e. g. at 0.01, 1.7, 4.2, 6.0, 6.7 and 9.5 cal. ka BP in the  $\delta^{18}\text{O}_{\text{diatom}}$  record roughly  
649 correspond to maxima in the biogenic opal concentration (Fig. 6). Some of these  $\delta^{18}\text{O}_{\text{diatom}}$   
650 minima are related to maxima (e. g. at 0.01, 6.0 cal. ka BP) in the total amount of lotic  
651 chironomids (Fig. 6).

652 Despite lower frequency variations of biogenic opal compared to  $\delta^{18}\text{O}_{\text{diatom}}$  and the absence  
653 of a statistically significant relationship between both, the transport of nutrients by inflow  
654 processes (by meltwaters) to the lake seems to be reflected in  $\delta^{18}\text{O}_{\text{diatom}}$ . The only other biotic  
655 proxy displaying a few similar, although not well-expressed maxima (i. e. at ~8.0, 6.4 and 2.0  
656 cal. ka BP) is the TOC record as proxy for organic matter deposition of Lake Bolshoye  
657 Shchuchye (Lenz et al., 2021).

658 A recent study by Cowling et al. (2021) deduced changes in the summer water balance and  
659 moisture sources during deglaciation and Early Holocene, using leaf wax hydrogen isotopes at  
660 Lake Bolshoye Shchuchye. However, a significant enrichment of  $\delta^2\text{H}_{\text{leaf wax}}$  values between  
661 10.5 and 10.0 cal. ka BP does not correspond to the changes in the  $\delta^{18}\text{O}_{\text{diatom}}$  signal (Fig. 4).  
662 This inconsistency can be related to uncertainties in the age models and temporal resolution of  
663 the datasets. Moreover, leaf waxes are related to (soil) water uptake into terrestrial and aquatic  
664 plants and more complicated for deriving the lake water isotope composition.

665 If we attribute the  $\delta^{18}\text{O}_{\text{diatom}}$  fluctuations to glacial advances, they should also be reflected in  
666 abiotic proxies such as clay content or Ti cps at Lake Bolshoye Shchuchye, which were  
667 interpreted as indicators for glacial meltwater input and catchment erosion, respectively (Lenz  
668 et al., 2021). Although there is a similarity between these abiotic parameters in the Holocene,  
669 they are neither reflecting a similar overall trend, nor similar short-term variations as found in  
670 the  $\delta^{18}\text{O}_{\text{diatom}}$  record.

671 Consequently, the hydrological changes inferred from the diatom isotopes have no clear  
672 linkage to the abiotic changes in the lake sediments, or these lake-internal proxies are not  
673 sensitive enough to record them. Hence, neither changes in glacial meltwater fluxes nor erosion

674 levels in the catchment (as inferred from Ti cps and clay contents) can explain the short-term  
675  $\delta^{18}\text{O}_{\text{diatom}}$  variability. This suggests that glaciers in the catchment, if present in the Holocene,  
676 were either too small or too distant from the lake to have a major influence on the sediment  
677 record. Hence, the only water source that can plausibly explain the short-term fluctuations in  
678 the record are changes in the snow and its meltwater supply in the catchment, independent from  
679 glacier-derived meltwater.

680

#### 681 5.6. Snow as key driver for short-term $\delta^{18}\text{O}_{\text{diatom}}$ fluctuations

682 Topographical features in the Polar Urals include leeward accumulation caused by persistent  
683 westerly winds, snow avalanches and shadowing-effects from mountain ridges. These factors can  
684 lead to a substantial (5–6 times, in the period 1958–1978) increase of the mean winter mass  
685 balance as compared to local precipitation (Mangerud et al., 2008). Presently, enhanced snow  
686 accumulation is strongly favored at higher elevations, on leeward slopes and in depressions  
687 (Voloshina, 1988). We draw the following conclusions from regional glacier mass balance  
688 studies: (1) the hydrology of the Polar Urals is strongly dominated by snow; (2) redistribution of  
689 snow may lead to a much higher SWE than actual precipitation (3) shadowing effects protect  
690 cirque glaciers and nival niches.

691 Figure 6 displays the geomorphological and snow characteristics of the Lake Bolshoye  
692 Shchuchye catchment. The DEM in Fig. 6A and the derived slopes angles in Fig. 6B reveal  
693 steeply (up to  $65^\circ$ ) incised valleys and several small streams draining into the lake. Generally,  
694 the catchment extends to the northwest of the lake with a maximum and mean elevation of about  
695 1200 and 500 m a.s.l., respectively.

696 For calculating the snow distribution of the Lake Bolshoye Shchuchye catchment we used  
697 the precipitation amount from snow profiles of the nearby Bol'shaya Khadata catchment  
698 (Gokhman & Zhidkov, 1979). Redistribution of snow may lead to a surplus of snow (reaching up  
699 to 8.45 m in snow height corresponding 3.40 m of snow-water equivalent; Figs 6 C and D) in

700 some areas of the catchment, especially in the higher altitudes and in narrow valleys in the  
701 northern/northwestern part of the catchment (Fig. 6). This suggests that in colder years, perennial  
702 snow fields may develop in leeward positions, storing the a surplus accumulated snow and  
703 allowing for increased snow melt contribution in warmer years.

704 These specific regional characteristics described above must necessarily have an impact on  
705 the lake hydrology, even though there are currently no glaciers in the Bolshoye Shchuchye  
706 catchment (Fig. 1B). As pointed out, a direct impact of glacier advances and retreat in the  
707 catchment in the Holocene is unlikely as abiotic indicators in the Holocene lake sediments do not  
708 suggest abrupt changes of sediment sources.

709 We therefore assume snow changes within the catchment to be the main driver of the  
710 catchment's hydrology and, thus, responsible for the short-term fluctuations in the  $\delta^{18}\text{O}_{\text{diatom}}$   
711 record. Due to shadowing effects, only part of this snow melts in summer and discharges into the  
712 lake. In phases of stronger winds and/or more precipitation, the Bolshoye Shchuchye catchment  
713 on the leeward side of the Polar Urals can receive excess snow amounts. While the exact  
714 mechanisms of how the snow and the snow melt affect the lake are yet to be identified, two  
715 dominating effects can be assumed: (1) more snow precipitation and redistribution directly lead  
716 to more snow in the catchment, and hence, possibly to a higher snow-derived and isotopically-  
717 depleted influx to the lake, (2) a local warming and/or reduced shadowing effect (Mangerud et  
718 al., 2008) may provide more snow melt to the lake, especially when the catchment is snow-  
719 saturated.

720 Enhanced snow influx hence directly impacts on the lake water isotopic composition when  
721 more melt waters from higher altitudes with lighter isotopic composition are drained to the lake.  
722 Conversely, centennial-scale maxima as observed in the Bolshoye Shchuchye diatom oxygen  
723 isotope record could be attributed to short-term interruptions of snow melt supply to the lake due  
724 to reduced influx from higher altitudes, and hence, lead to isotopically heavier  $\delta^{18}\text{O}_{\text{diatom}}$  values.  
725 The quick rebounds towards isotopically lighter values may then reflect a return to the "normal"

726 conditions prevailing before these excursions: large amounts of snow being redistributed from  
727 the windward side of the Polar Urals towards the leeward side (into the Bolshoye Shchuchye  
728 catchment).

729 In summary, the complex interplay between local hydroclimatic conditions with more snow  
730 delivered to the catchment (more P, stronger winds) and temporarily enhanced snow-melt phases  
731 (higher summer T) likely drives the observed short-term changes in the Bolshoye Shchuchye  
732 catchment. This mechanism allows for using the Bolshoye Shchuchye diatom oxygen isotopes as  
733 local snow-melt indicator, hence as paleo precipitation and summer temperature proxy.

734

## 735 **6. Conclusions**

736 Lake Bolshoye Shchuchye is a well-mixed lake, covered by ice for more than half of the  
737 year, with negligible evaporative effects, as derived from the recent water isotope dataset.  
738 Diatom oxygen isotopes ( $\delta^{18}\text{O}_{\text{diatom}}$ ) from the lacustrine sediments of Lake Bolshoye Shchuchye  
739 have been used as proxies for the hydrological and climate dynamics in the lake catchment.  
740 During the Holocene, the Lake Bolshoye Shchuchye  $\delta^{18}\text{O}_{\text{diatom}}$  record generally follows a  
741 decrease in summer insolation, in line with the northern hemisphere (NH) temperature history.  
742 However, Lake Bolshoye Shchuchye displays exceptional, short-term, centennial-scale changes  
743 of exceeding 5‰, especially in Mid and Late Holocene contemporaneous with and similar to NH  
744 glacier advances. As most of these minima and maxima are confirmed by more than one data  
745 point, these are considered as no methodological artefacts. Mixing calculations reveal that ~ 30–  
746 50% of the Lake Bolshoye Shchuchye water needs to be exchanged with isotopically different  
747 water within short time to account for these shifts in  $\delta^{18}\text{O}_{\text{diatom}}$ . However, larger Holocene glacier  
748 advances in the Lake Bolshoye Shchuchye catchment are not known and have left no significant  
749 imprint on the lakes' abiotic proxies. Accordingly, a source of light isotope composition is snow,  
750 known to be transported in significant quantities and with large variability to the leeward side of  
751 the Polar Urals. Hence, we consider snow transport to the catchment and switch on/off of

752 meltwater supply to the lake as dominant hydrological process responsible for the observed  
753 short-term changes in the  $\delta^{18}\text{O}_{\text{diatom}}$  record. A linkage between meltwater influx to lakes and  
754  $\delta^{18}\text{O}_{\text{diatom}}$  has been found before (Meyer et al., 2015). Here, however, centennial-scale  
755 hydrological changes have been documented in this high-latitude diatom oxygen isotope record,  
756 which, for this specific setting, are interpreted as indicator for palaeo precipitation and summer  
757 temperature changes.

758

### 759 **Acknowledgements**

760 The study was performed in the frame of the German-Russian projects ‘PLOT –  
761 Paleolimnological Transect’ (BMBF; grant 03G0859) and its successor ‘PLOT – Synthesis’  
762 (BMBF; grant 03F0830C) both funded by the German Federal Ministry of Education and  
763 Research. We thank Ilona Schaepan from the German Research Center for Geosciences (GFZ) in  
764 Potsdam for the EDX analyses, Rita Fröhlking-Teichert from the AWI Bremerhaven Marine  
765 Geology laboratory for BSi measurements, and Mikaela Weiner for technical support during  
766 sample preparation and isotope measurements at the AWI Potsdam stable isotope laboratory.  
767 Topographic and snow redistribution analyses were performed with support of the RUDN  
768 University Strategic Academic Leadership Program (Dr. Yuri Dvornikov).

769

### 770 **References**

- 771 Andreev, A.A., Tarasov, P.E., Ilyashuk, B.P., Ilyashuk, E.A., Cremer, H., Hermichen, W.-D.,  
772 Wischer, F., Hubberten, H.-W. (2005). Holocene environmental history recorded in Lake  
773 Lyadhej-To sediments, Polar Urals, Russia. *Palaeogeography, Palaeoclimatology,*  
774 *Palaeoecology*, 223, 181–203.
- 775 Astakhov, V.I. (2018). Late Quaternary glaciation of the northern Urals: a review and new  
776 observations. *Boreas* 47, 379–389.
- 777 Berger, A., Loutre, M.F. (1991). Insolation values for the climate of the last 10 million years.  
778 *Quaternary Science Reviews* 10, 297–317.
- 779 Biskaborn, B. K., Nazarova, L., Pestryakova, L. A., Syrykh, L., Funck, K., Meyer, H.,  
780 Chaplignin, B., Vyse, S., Gorodnichev, R., Zakharov, E., Wang, R., Schwamborn, G., and

781 Diekmann, B. (2019). Spatial distribution of environmental indicators in surface sediments of  
782 Lake Bolshoe Toko, Yakutia, Russia, *Biogeosciences* 16(20), 4023-4049.  
783 <https://doi.org/10.5194/bg-2019-146>.

784 Blaauw, M. (2010). Methods and code for 'classical' age-modelling of radiocarbon  
785 sequences. *Quaternary Geochronology* 5: 512-518.

786 Blaauw, M. (2021). Clam: Classical Age-Depth Modelling of Cores from Deposits. R  
787 package version 2.3.9.

788 Bogdanov, V.D., Bogdanova, E.N., Gavrillov, A.L., Melnichenko, I.P., Stepanov, L.N.,  
789 Yarushina, M.I. (2004). Biological resources of aquatic ecosystems of the Polar Urals.  
790 Publishing House of Ural Branch of RAS, Ekaterinburg. 168 pp. (in Russian).

791 Bonne, J.-L., Meyer, H., Behrens, M., Boike, J., Kipfstuhl, S., Rabe, B., Schmidt, T.,  
792 Schönicke, L., Steen-Larsen, H. C., Werner, M., (2020). Moisture origin as a driver of temporal  
793 variabilities of the water vapour isotopic composition in the Lena River Delta, Siberia.  
794 *Atmospheric Chemistry and Physics*, 20(17), 10493–10511. [https://doi.org/10.5194/acp-20-](https://doi.org/10.5194/acp-20-10493-2020)  
795 10493-2020

796 Bowen, G.J. (2021). The Online Isotopes in Precipitation Calculator, version OIPC3.1  
797 (4/2017) <http://www.waterisotopes.org>

798 Bowen, G.J., & Revenaugh, J. (2003). Interpolating the isotopic composition of modern  
799 meteoric precipitation. *Water Resources Research* 39 (10), 1299. doi:10.129/2003WR002086.

800 Bowen, G.J., Wassenaar, L.I., Hobson, K.A. (2005). Global application of stable hydrogen  
801 and oxygen isotopes to wildlife forensics. *Oecologia* 143, 337–348.

802 Brooks, S.J., Langdon, P.G., Heiri, O. (2007). The identification and use of palaeartic  
803 chironomidae larvae in palaeoecology. QRA Technical Guide No. 10. Quaternary Research  
804 Association, London. 276 pp.

805 Cartier, R., Sylvestre, F., Paillès, C., Sonzogni, C., Couapel, M., Alexandre, A., Mazur, J.-C.,  
806 Brisset, E., Miramont, C., Guiter, F. (2019). Diatom-oxygen isotope record from high-altitude  
807 Lake Petit (2200 m a.s.l.) in the Mediterranean Alps: shedding light on a climatic pulse at 4.2 ka.  
808 *Climate of the Past* 15, 253–263.

809 Chaplignin, B., Leng, M.J., Webb, E., Alexandre, A., Dodd, J.P., Ijiri, A., Lücke, A.,  
810 Shemesh, A., Abelman, A., Herzsuh, H., Longstaffe, F.J., Meyer, H., Moschen, R., Okazaki,  
811 Y., Rees, N.H., Sharp, Z.D., Sloane, H.J., Sonzongi, C., Swann, J.E.A., Sylvestre, F., Tyler, J.J.,  
812 Yam, R. (2011). Inter-laboratory comparison of oxygen isotope compositions from biogenic  
813 silica. *Geochimica et Cosmochimica Acta* 75, 7242–7256.

814 Chaplign, B., Meyer, H., Bryan, A., Snyder, J., Kemnitz, H. (2012a). Assessment of  
815 purification and contamination correction methods for analysing the oxygen isotope composition  
816 from biogenic silica. *Chemical Geology* 300–301, 185–199.

817 Chaplign, B., Meyer, H., Friedrichsen, H., Marent, A., Sohns, E., Hubberten, H.-W. (2010).  
818 A high-performance, safer and semi-automated approach for the  $\delta^{18}\text{O}$  analysis of diatom silica  
819 and new methods for removing exchangeable oxygen. *Rapid Communications in Mass*  
820 *Spectrometry* 24, 2655–2664.

821 Chaplign, B., Meyer, H., Swann, G.E.A., Meyer-Jacob, C., Hubberten, H.-W. (2012b). A  
822 250-ka oxygen isotope record from diatoms at Lake El'gygytyn, far east Russian Arctic.  
823 *Climate of the Past*, 8, 1621–1636. <https://doi.org/10.5194/cp-8-1621-2012>.

824 Clarke, C.L., Alsos, I.G., Edwards, M.E., Paus, A., Gielly, L., Haflidason, H., Mangerud, J.,  
825 Regnéll, C., Hughes, P.D.M., Svendsen, J.I., Bjune, A.E. (2020). A 24,000-year ancient DNA  
826 and pollen record from the Polar Urals reveals temporal dynamics of arctic and boreal plant  
827 communities. *Quaternary Science Reviews*, 247, 106564.

828 Clayton, R., & Mayeda, T. (1963). The use of bromine pentafluoride in the extraction of  
829 oxygen from oxides and silicates for isotopic analysis. *Geochimica et Cosmochimica Acta*, 27,  
830 43–52.

831 Cowling, O., Thomas, E., Svendsen, J.I., Mangerud, J., Haflidason, H., Regnéll, C.,  
832 Brendryen, J. (2021). The hydrologic cycle in western Siberia during the past 24,000 years  
833 changed in step with plant community structure. *Journal of Quaternary Science*.

834 Craig, H. (1961). Isotopic variations in meteoric waters. *Science* 133, 1702–1703.

835 Cremer, H., Andreev, A., Hubberten, H.-W., Wischer, F. (2004). Paleolimnological  
836 reconstructions of Holocene environments and climate from Lake Lyadhej-To, Ural Mountains,  
837 Northern Russia. *Arctic, Antarctic, and Alpine Research*, 36, 147– 155.

838 Dahl, S.O., Bakke, J., Lie, Ø., Nesje, A. (2003). Reconstruction of former glacier  
839 equilibrium-line altitudes based on proglacial sites: an evaluation of approaches and selection of  
840 sites. *Quaternary Science Reviews*, 22, 275–287.

841 Dansgaard, W. (1964). Stable isotopes in precipitation. *Tellus*, 16 (4), 436–468.

842 Davis, P.T., Menounos, B., Osborn, G. (2009). Holocene and latest Pleistocene alpine glacier  
843 fluctuations: a global perspective. *Quaternary Science Reviews*, 28, 2021–2033.

844 Darling, W.G., Bath, A.H., Gibson, J.J., Rozanski, K. (2006). Isotopes in Water. In: Leng  
845 M.J. (Ed.). *Isotopes in Paleoenvironmental Research*. Vol. 10. Springer, Dordrecht, pp. 1-52.

846 Dodd, J.P., & Sharp, Z.D. (2010). A laser fluorination method for oxygen isotope analysis of  
847 biogenic silica and a new oxygen isotope calibration of modern diatoms in freshwater  
848 environments. *Geochimica et Cosmochimica Acta*, 74, 1381–1390.

849 Dortch, J.M., Owen, L.A., Caffee, M.W. (2013). Timing and climatic drivers for glaciation  
850 across semi-arid western Himalayan-Tibetan orogen. *Quaternary Science Reviews*, 78,188–208.

851 Dushin, V.A., Serdyukova, O.P., Malyugin, A.A., Nikulina, I.A., Kozmin, V.S., Burmako,  
852 P.L., Abaturova, I.V., Kozmina, L.I. (2009). State Geological Map of the Russian Federation  
853 1:200000. Polar Ural Series. Sheet Q-42-I, II (Laborovaya). VSEGEI, St. Petersburg (in  
854 Russian).

855 Dvornikov, Y. A., Khomutov, A. V., Mullanurov, D. R., Ermokhina, K. A., Gubarkov, A. A.,  
856 & Leibman, M. O. (2015). GIS and field data based modelling of snow water equivalent in shrub  
857 tundra. *Fennia*, 193(1), 53–65. <https://doi.org/10.11143/46363>

858 Evans, J. S. (2020). *R spatialEco-package* (1.3-1). <https://github.com/jeffrejevans/spatialEco>

859 Friedman, I., Benson, C., Cleason, J. (1991). Isotopic changes during snow metamorphism.  
860 In H.P. Taylor, J.R. O’Neil, I.R. Kaplan (Eds.) *Stable Isotope Geochemistry: A Tribute to*  
861 *Samuel Epstein* (pp. 211–221). The Geochemical Society. Special Publication No. 3.

862 Gardner, A.S., Moholdt, G., Cogley, J.G., Wouters, B., Arendt, A.A., Wahr, J., Berthier, E.,  
863 Hock, R., et al. (2013). A reconciled estimate of glacier contributions to sea level rise: 2003 to  
864 2009. *Science*, 340, 852–857.

865 Gat, J.R. (1981). Lakes. In: Gat, J.R. and Gonfiantini, R. (Eds.). *Stable Isotope Hydrology -*  
866 *Deuterium and Oxygen-18 in the water cycle*. Tech. Rep. Series No. 210. IAEA, Vienna, pp.  
867 203-221.

868 Gibson, J.J., Edwards, T.W.D. and Prowse, T.D (1999). Pan-derived isotopic composition of  
869 atmospheric water vapour and its variability in northern Canada. *Journal of Hydrology*, 217, 55-  
870 74.

871 Gibson, C.E., Anderson, N.J., Haworth, E.Y. (2003). *Aulacoseira subarctica*: taxonomy,  
872 physiology, ecology and palaeoecology. *European Journal Phycology*, 38, 83–101.

873 Gokhman, V. V., & Zhidkov, V. A. (1979). On the spatial distribution of snow storage in  
874 Polar Urals. In V. M. Kotlyakov (Ed.), *Data of glaciological studies* (pp. 177–182). Academy of  
875 Sciences USSR.

876 Gonfiantini R. (1986). Environmental isotopes in Lake Studies. In: Fritz, O. and Fontes, J.C.  
877 (Eds.). *Handbook of environmental isotope Geochemistry: Vol 2, The Terrestrial Environment*,  
878 B. Elsevier, Amsterdam, pp. 113-168.

879 Gorelick, N., Hancher, M., Dixon, M., Ilyushchenko, S., Thau, D., & Moore, R. (2017).  
880 Google Earth Engine: Planetary-scale geospatial analysis for everyone. *Remote Sensing of*  
881 *Environment*, 202, 18–27. <https://doi.org/10.1016/J.RSE.2017.06.031>

882 Haflidason, H., Zweidorff, J.L., Baumer, M., Gyllencreutz, R., Svendsen, J.I., Gladyshev, V.,  
883 Logvina, E. (2019). The Lastglacial and Holocene seismostratigraphy and sediment distribution  
884 of Lake Bolshoye Shchuchye, Polar Ural Mountains, Arctic Russia. *Boreas*, 48, 452–469.

885 Heikkilä, M., Edwards, T.W.D., Seppä, H., Sonninen, E. (2010). Sediment isotope tracers  
886 from Lake Saarikko, Finland, and implications for Holocene hydroclimatology. *Quaternary*  
887 *Science Reviews*, 29, 17–18, 2146–2160. <https://doi.org/10.1016/j.quascirev.2010.05.010>.

888 Huggel, C., Haeberli, W., Kääh, A. (2008). Glacial hazards: perceiving and responding to  
889 threats in four world regions. In: Orlove, B., Wiegandt, E., Luckman, B.H. (Eds.). *Darkening*  
890 *peaks. Glacier retreat, science and society*. University of California Press, Berkeley, US. 68–80.

891 Hutchinson, M. F. (1989). A new procedure for gridding elevation and stream line data with  
892 automatic removal of spurious pits. *Journal of Hydrology*, 106, 211–232.  
893 [https://doi.org/10.1016/0022-1694\(89\)90073-5](https://doi.org/10.1016/0022-1694(89)90073-5)

894 IAEA/WMO (2021). Global Network of Isotopes in Precipitation. The GNIP Database.  
895 <https://nucleus.iaea.org/wiser>

896 IPCC (2014). Climate Change 2014: Synthesis Report. Contribution of Working Groups I, II  
897 and III to the Fifth Assessment Report of the Intergovernmental Panel on Climate Change [Core  
898 Writing Team, R. K. Pachauri, & L. A. Meyer (Eds.)]. Latest Pleistocene and Holocene glacier  
899 variations in the European Alps. *Quaternary Science Reviews*, 28, 2137–2149.

900 Ivanov, M. N. (2013). *Evolution of glaciation of the Polar Urals in the late Holocene* (A. A.  
901 Lukashov & E. S. Troshkina (eds.)). Faculty of Geography, MSU.

902 Ivy-Ochs, S., Kerschner, H., Maisch, M., Christl, M., Kubik, P.W., Schluechter, C. (2009).  
903 Latest Pleistocene and Holocene glacier variations in the European Alps. *Quaternary Science*  
904 *Reviews*, 28, 2137–2149.

905 Jankovská, V., Andreev, A.A., Panova, N.K. (2006). Holocene environmental history on the  
906 eastern slope of the Polar Ural Mountains, Russia. *Boreas*, 35, 650–661.

907 Juillet-Leclerc, A., & Labeyrie, L. (1987). Temperature dependence of the oxygen isotopic  
908 fractionation between diatom silica and water. *Earth and Planetary Science Letters*, 84, 69–74.

909 Jones, V. J., Leng, M. J., Solovieva, N., Sloane, H. J. & Tarasov, P. (2004). Holocene climate  
910 of the Kola Peninsula; evidence from the oxygen isotope record of diatom silica. *Quaternary*  
911 *Science Reviews*, 23, 833–839.

912 Kemmerich, A.O. (1966). *The Polar Urals*. Publishing House Fizkultura i Sport, Moscow.  
913 112 pp. (in Russian).

914 Koboltschnig, G.R., & Schöner, W. (2011). The relevance of glacier melt in the water cycle  
915 of the Alps: the example of Austria. *Hydrology and Earth System Sciences*, 15, 2039–2048.

916 Kononov, Y.M., Ananicheva, M.D., Willis, I.C. (2005). High-resolution reconstruction of  
917 Polar Ural glacier mass balance for the last millennium. *Annals of Glaciology*, 42, 163–170.

918 Kostrova, S.S., Biskaborn, B.K., Pestryakova, L.A., Fernandoy, F., Lenz, M.M., Meyer, H.,  
919 (2021). Climate and environmental changes of the Lateglacial transition and Holocene in  
920 northeastern Siberia: Evidence from diatom oxygen isotopes and assemblage composition at  
921 Lake Emanda. *Quaternary Science Reviews*, 259, 106905. [https://doi.org/10.1016/  
922 j.quascirev.2021.106905](https://doi.org/10.1016/j.quascirev.2021.106905)

923 Kostrova, S.S., Meyer, H., Bailey, H.L., Ludikova, A.V., Gromig, R., Kuhn, G., Shibaev,  
924 Y.A., Kozachek, A.V., Ekaykin, A.A., Chapligin, B. (2019). Holocene hydrological variability  
925 of Lake Ladoga, northwest Russia, as inferred from diatom oxygen isotopes. *Boreas*, 48, 361–  
926 376.

927 Kostrova, S.S., Meyer, H., Chapligin, B., Kossler, A., Bezrukova, E.V., Tarasov, P.E. (2013).  
928 Holocene oxygen isotope record of diatoms from Lake Kotokel (southern Siberia, Russia) and its  
929 palaeoclimatic implications. *Quaternary International*, 290–291, 21–34.

930 Kostrova, S.S., Meyer, H., Chapligin, B., Tarasov, P.E., Bezrukova, E.V. (2014). The last  
931 glacial maximum and late glacial environmental and climate dynamics in the Baikal region  
932 inferred from an oxygen isotope record of lacustrine diatom silica. *Quaternary International*,  
933 348, 25–36.

934 Khromova, T., Nosenko, G., Kutuzov, S., Muraviev, A., Chernova, L. (2014). Glacier area  
935 changes in Northern Eurasia. *Environmental Research Letters*, 9, 015003.

936 Khromova, T., Nosenko, G., Nikitin, S., Muraviev, A., Popova, V., Chernova, L., Kidyayeva,  
937 V. (2019). Changes in the mountain glaciers of continental Russia during the twentieth to  
938 twenty-first centuries. *Regional Environmental Change*, 19, 1229–1247.

939 Labeyrie, L.D. (1974). New approach to surface seawater palaeotemperatures using  $^{18}\text{O}/^{16}\text{O}$   
940 ratios in silica of diatom frustules. *Nature*, 248, 40–42.

941 Lammers, Y., Clarke, C.L., Erséus, C., Brown, A.G., Edwards, M.E., Gielly, L., Haflidason,  
942 H., Mangerud, J., Rota, E., Svendsen, J.I., Alsos, I.G. (2019). Clitellate worms (Annelida) in  
943 lateglacial and Holocene sedimentary DNA records from the Polar Urals and northern Norway.  
944 *Boreas*, 48, 317–329.

945 Lawrence, M. (2005). The Relationship between Relative Humidity and the Dewpoint  
946 Temperature in Moist Air: A Simple Conversion and Applications. *Bulletin of the American  
947 Meteorological Society*, 86, 225–233.

948 Leng, M.J., & Barker, P.A. (2006). A review of the oxygen isotope composition of lacustrine  
949 diatom silica for palaeoclimate reconstruction. *Earth-Science Reviews*, 75, 5–27.

950 Lenz, M. M., Andreev, A., Nazarova, L., Syrykh, L.S., Scheidt, S., Haflidason, H., Meyer,  
951 H., Brill, D., Wagner, B., Gromig, R., N., Lenz, M., Rolf, C., Kuhn, G., Fedorov, G., Svendsen,  
952 J.I., Melles, M. (2021). Climate and environmental history of the Polar Ural Mountains since  
953 early MIS 2 inferred from a 54-m-long sediment core from Lake Bolshoye Shchuchye. *Journal*  
954 *of Quaternary Science*. DOI: 10.1002/jqs.3400.

955 Lepskaya, E.V., Jewson, D.H., Usoltseva, M.V. (2010). *Aulacoseira subarctica* in  
956 Kurilskoye Lake, Kamchatka: A deep, oligotrophic lake and important pacific salmon nursery.  
957 *Diatom Research*, 25 (2), 323–335.

958 Linacre, E. T. (1977). A simple formula for estimating evaporation rates in various climates,  
959 using temperature data alone. *Agric. Meteorol.*, 18, 409–424.

960 Lubinsky, D.J., Forman, S.L., Miller, G.H. (1999). Holocene glacier and climate fluctuations  
961 on Franz Josef Land, Arctic Russia, 80° N. *Quaternary Science Reviews*, 18 (1), 85–108.

962 Mangerud, J., Gosse, J., Matiouchkov, A., Dolvik, T. (2008). Glaciers in the Polar Urals,  
963 Russia, were not much larger during the Last Global Glacial Maximum than today. *Quaternary*  
964 *Science Reviews*, 27, 1047–1057.

965 Matthews, J.A., Dresser, P.Q. (2008). Holocene glacier variation chronology of the  
966 Smørstabbtinden massif, Jotunheimen, southern Norway, and the recognition of century- to  
967 millennial-scale European Neoglacial events. *Holocene*, 18, 181–201.

968 Meyer, H., Chaplignin, B., Hoff, U., Nazarova, L., Diekmann, B. (2015). Oxygen isotope  
969 composition of diatoms as Late Holocene climate proxy at Two-Yurts Lake, Central Kamchatka,  
970 Russia. *Global and Planetary Change*, 134, 118–128.

971 Meyer, H., Schönicke, L., Wand, U., Hubberten, H.-W., Friedrichsen, H. (2000). Isotope  
972 studies of hydrogen and oxygen in ground ice – experiences with the equilibration technique.  
973 *Isotopes in Environmental and Health Studies*, 36, 133–149.

974 Mitrofanova, E.Y. (2017). Phytoplankton of the Lake Bolshoe Shchuchye and rivers of its  
975 basin in August 2016. Scientific Newsletter of Yamalo-Nenets Autonomous Region 1 (94),  
976 55–61 (in Russian).

977 Moller Pillot, H.K.M. (2009). Chironomidae Larvae. Biology and ecology of the  
978 Chironomini. KNNV Publishing, Zeist. 270 pp.

979 Moller Pillot H.K.M. (2013). Chironomidae larvae of the Netherlands and adjacent lowlands.  
980 Volume 3 Biology and ecology of the aquatic Orthocladinae. 312 pp. KNNV Publishing, Zeist,  
981 Netherlands.

982 Morozova, L.M., Magomedova, M.A., Ektova, S.N., Dyachenko, A.P., Knyazev., M.S.  
983 (Eds.), 2006. Vegetation cover and plant resources of the Polar Urals. Publishing House of the  
984 Ural University, Yekaterinburg. 796 pp. (in Russian).

985 Mortlock, R.D., & Froelich, P.N. (1989). A simple method for the rapid determination of  
986 biogenic opal in pelagic marine sediments. *Deep-Sea Research*, 36, 1415–1426.

987 Müller, P.J., & Schneider, R. (1993). An automated leaching method for the determination of  
988 opal in sediments and particulate matter. *Deep Sea Research Part I*, 40, 425–444.

989 Nazarova, L., Bleibtreu, A., Hoff, U., Dirksen, V., Diekmann, B. (2017a). Changes in  
990 temperature and water depth of a small mountain lake during the past 3000 years in Central  
991 Kamchatka reflected by chironomid record. *Quaternary International*, 447, 46–58.

992 Nazarova, L., Herzsuh, U., Wetterich, S., Kumke, T., Pestjakova, L. (2011). Chironomid-  
993 based inference models for estimating mean July air temperature and water depth from lakes in  
994 Yakutia, northeastern Russia. *Journal of Paleolimnology*, 45, 57–71.

995 Nazarova, L., Self, A., Brooks, S.J., van Hardenbroek, M., Herzsuh, U., Diekmann, B.  
996 (2015). Northern Russian chironomid-based modern summer temperature data set and inference  
997 models. *Global Planetary Change*, 134, 10–25.

998 Nazarova, L.B., Self, A.E., Brooks, S.J., Solovieva, N., Syrykh, L.S., Dauvalter, V.A.  
999 (2017b). Chironomid Fauna of the Lakes from the Pechora River Basin (East of European part of  
1000 Russian Arctic): Ecology and Reconstruction of Recent Ecological Changes in the Region.  
1001 *Contemporary Problems of Ecology*, 10, 350–362.

1002 Nazarova L., Grebennikova T.A., Razjigaeva N.G., Ganzey L.A., Belyanina N.I., Arslanov  
1003 K.A., Kaistrenko V.M., Gorbunov A.O., Kharlamov A.A., Rudaya N., Palagushkina O.,  
1004 Biskaborn B.K., Diekmann B. (2017c). Reconstruction of Holocene environmental changes in  
1005 Southern Kurils (North-Western Pacific) based on palaeolake sediment proxies from Shikotan  
1006 Island. *Global and Planetary Change*, 159: 25–36. DOI: 10.1016/j.gloplacha.2017.10.005

1007 Nazarova, L., Sachse D., Fuchs H.G.E., Dirksen V., Dirksen O., Syrykh L., Razjigaeva N.G.,  
1008 Diekmann B. (2021a). Holocene evolution of a proglacial lake in southern Kamchatka, Russian  
1009 Far East. *Boreas* doi: 10.1111/bor.12554

1010 Nazarova L., Frolova L.A., Palagushkina O.V., Rudaya N.A., Syrykh L.S., Grekov I.M.,  
1011 Solovieva N., O.A. Loskutova O.A. (2021b). Recent shift in biological communities: A case  
1012 study from the Eastern European Russian Arctic (Bol'shezemelskaya Tundra). *Polar biology*.  
1013 doi: 10.1007/s00300-021-02876-7

1014 Nesje, A. (2009). Latest Pleistocene and Holocene alpine glacier fluctuations in Scandinavia.  
1015 *Quaternary Science Reviews*, 28, 2119–2136.

1016 Nesje, A., Bakke, J., Brooks, S.J., Kaufman, D.S., Kihlberg, E., Trachsel, M., D'Andrea,  
1017 W.J., Matthews, J.A. (2014). Late glacial and Holocene environmental changes inferred from  
1018 sediments in Lake Myklevatnet, Nordfjord, western Norway. *Vegetation History and*  
1019 *Archaeobotany*, 23, 229–248.

1020 Nikolaev, V.I., & Mikhalev, D.V. (1995). An oxygen-isotope paleothermometer from ice in  
1021 Siberian permafrost. *Quaternary Research*, 43, 14–21.

1022 NOAA NCEI, (2021). NOAA National Centers for Environmental Information. State of the  
1023 climate: Global climate report for April 2020, published online May 2020, retrieved on May 26,  
1024 2020. <https://www.ncdc.noaa.gov/sotc/global/202004>

1025 Nosenko, G., & Tsvetkov, D. (2003). Assessment of glaciers change on Polar Urals from  
1026 ASTER imagery. In: Glaciological data. Report GD-32. National Snow and Ice Data Center,  
1027 Boulder. 80–82.

1028 Panova, N.K., Jankovska, V., Korona, O.M., Zinov'ev, E.V. (2003). The Holocene dynamics  
1029 of vegetation and ecological conditions of the Polar Urals. *Russian Journal of Ecology*, 34, 219–  
1030 230.

1031 Pechkin, A.S., Kirillov, V.V., Koveshnikov, M.I., Krasnenko, A.S., Saltykov, A.V., Timkin,  
1032 A.V., Dyachenko, A.V., (2017). Morphometric characteristics of the Lake Bolshoe Shchuchye.  
1033 Scientific Newsletter of Yamalo-Nenets Autonomous Region 3 (96), 48–52 (in Russian).

1034 Petrakov, D.A., Chernomorets, S.S., Evans, S.G., Tutubalina, O.V. (2008). Catastrophic  
1035 glacial multi-phase mass movements: a special type of glacial hazard. *Advances in Geosciences*,  
1036 14, 211–218.

1037 Pischalnikova, E.V. (2016). Circulation conditions of abundant snowfalls formation in Perm  
1038 region. *Geographical bulletin*, 1 (36). 70–77 (in Russian).

1039 Porter, C., Morin, P., Howat, I., Noh, M.-J., Bates, B., Peterman, K., Keeseey, S., Schlenk,  
1040 M., Gardiner, J., Tomko, K., et al. (2018). *ArcticDEM*. Harvard Dataverse, V1.  
1041 <https://doi.org/10.7910/DVN/OHHUKH>

1042 Quinn, P., Beven, K. J., & Lamb, R. (1995). The In (a/tan/beta) index: How to calculate it  
1043 and how to use it within the Topmodel framework. *Hydrological Processes*, 9(2), 161–182.

1044 R Core Team. (2017). R: A language and environment for statistical computing. R  
1045 Foundation for Statistical Computing. <https://www.r-project.org/>

1046 R Core Team. (2020). R: A language and environment for statistical computing. R  
1047 Foundation for Statistical Computing. <https://www.r-project.org/>

1048 Radić, V., & Hock, R. (2014). Glaciers in the Earth's hydrological cycle: Assessments of  
1049 glacier mass and runoff changes on global and regional scales. *Surveys in Geophysics* 35. 813–  
1050 837.

1051 Regnéll, C., Haflidason, H., Mangerud, J., Svendsen, J.I. (2019). Glacial and climate history  
1052 of the last 24 000 years in the Polar Ural Mountains, Arctic Russia, inferred from partly varved  
1053 lake sediments. *Boreas*, 48, 432–443.

1054 Robert, J. H., & van Etten, J. (2012). *R-package raster: Geographic analysis and modeling*  
1055 *with raster data* (2.0-12). <http://cran.r-project.org/package=raster>

1056 Rozanski, K., Araguás-Araguás, L., Gonfiantini, R. (1993). Isotopic patterns in modern  
1057 global precipitation. Geophysical Monograph 78. In *Climate Change in Continental Isotope*  
1058 *Records* (pp. 1–36). American Geophysical Union Monograph.

1059 Shahgedanova, M., Nosenko, G., Bushueva, I., Ivanov, M. (2012). Changes in area and  
1060 geodetic mass balance of small glaciers, Polar Urals, Russia, 1950–2008. *Journal of Glaciology*,  
1061 58 (211), 953–964.

1062 Shemesh, A., Rosqvist, G., Rietti-Shati, M., Rubensdotter, L., Bigler, C., Yam, R., Karlen,  
1063 W. (2001). Holocene climatic change in Swedish Lapland inferred from an oxygen-isotope  
1064 record of lacustrine biogenic silica. *Holocene*, 11 (4), 447–454.

1065 Solomina, O., Ivanov, M., Bradwell, T. (2010). Lichenometric studies on moraines in the  
1066 Polar Urals. *Geografiska Annaler: Series A, Physical Geography*, 92 (1), 81–99.

1067 Solomina, O.N., Bradley, R.S., Hodgson, D.A., Ivy-Ochs, S., Jomelli, V., Mackintosh, A.N.,  
1068 Nesje, A., Owen, L.A., Wanner, H., Wiles, G.C., Young, N.E. (2015). Holocene glacier  
1069 fluctuations. *Quaternary Science Reviews*, 111, 9–34.

1070 Solovieva N, Jones VJ., Birks HJB., Appleby PG., Nazarova L. (2008). Diatom responses to  
1071 20th century climate warming in lakes from the northern Urals, Russia. *Palaeogeography*,  
1072 *Palaeoclimatology, Palaeoecology*, 259: 96–106.

1073 Stief, P., Nazarova L., & De Beer D. (2005). Chimney construction by *Chironomus riparius*  
1074 larvae in response to hypoxia: microbial implications for freshwater sediments. *Journal of North*  
1075 *American Benthological Society*, 24 (4): 858-871.

1076 Svendsen, J. I., Alexanderson, H., Astakhov, V. I., Demidov, I., Dowdeswell, J. A., Funder,  
1077 S., Gataullin, V., Henriksen, et al. (2004). Late Quaternary ice sheet history of northern Eurasia.  
1078 *Quaternary Science Reviews*, 23 (11), pp. 1229-1272. doi: 10.1016/j.quascirev.2003.12.008

1079 Svendsen, J.I., Krüger, L.C., Mangerud, J., Astakhov, V.I., Paus, A., Nazarov, D., Murray,  
1080 A. (2014). Glacial and vegetation history of the Polar Ural Mountains in northern Russia during  
1081 the Last Ice Age, Marine Isotope Stages 5–2. *Quaternary Science Reviews*, 92, 409–428.

1082 Svendsen, J.I., Færseth, L.M.B., Gyllencreutz, R., Hafliðason, H., Henriksen, M., Hovland,  
1083 M.N., Lohne, Ø.S., Mangerud, J., et al. (2019). Glacial and environmental changes over the last  
1084 60 000 years in the Polar Ural Mountains, Arctic Russia, inferred from a high-resolution lake  
1085 record and other observations from adjacent areas. *Boreas*, 48, 407–431.

1086 Svensson, A., Andersen, K.K., Bigler, M., Clausen, H.B., Dahl-Jensen, D., Davies, S.M.,  
1087 Johnsen, S.J., Muscheler, R., et al., (2008). A 60.000 year Greenland stratigraphic ice core  
1088 chronology. *Climate of the Past*, 4, 47–57.

1089 Swann, G.E.A., Leng, M.J. (2009). A review of diatom  $\delta^{18}\text{O}$  in palaeoceanography.  
1090 *Quaternary Science Reviews*, 28, 384–398.

1091 Swann, G.E.A., Leng, M.J., Juschus, O., Melles, M., Brigham-Grette, J., Sloane, H.J. (2010).  
1092 A combined oxygen and silicon diatom isotope record of Late Quaternary change in Lake  
1093 El'gygytgyn, North East Siberia. *Quaternary Science Reviews*, 29, 774-786.  
1094 <https://doi.org/10.1016/j.quascirev.2009.11.024>.

1095 van Hardenbroek, M., Chakraborty, A., Davies, K.L., Harding, P., Heiri, O., Henderson,  
1096 A.C.G., Holmes, J.A., Lasher, G.E., et al., (2018). The stable isotope composition of organic and  
1097 inorganic fossils in lake sediment records: Current understanding, challenges, and future  
1098 directions. *Quaternary Science Reviews*, 196, 154–176.

1099 Vinokurova, G.V. (2017). Phytoepilithon of the Lake Bolshoe Shchuchye and rivers flowing  
1100 into and out of it (the Polar Urals). Scientific Newsletter of Yamalo-Nenets Autonomous Region  
1101 1 (94), 11–14 (in Russian).

1102 Voloshina, A. (1988). Some results of glacier mass balance research on the glaciers in the  
1103 Polar Urals. *Polar Geography and Geology*, 12, 200–211.

1104 Wiederholm, T. (1983). Chironomidae of the Holarctic Region, Keys and Diagnoses. Part 1.  
1105 Larvae: Entomologica Scandinavica, Supplement 19, 1–457.

1106 WGMS, (2017). Global Glacier Change Bulletin No. 2 (2014–2015). Zemp, M.,  
1107 Nussbaumer, S.U., Gärtner-Roer, I., Huber, J., Machguth, H., Paul, F., Hoelzle, M. (Eds.).  
1108 ICSU(WDS)/IUGG(IACS)/UNEP/UNESCO/WMO, World Glacier Monitoring Service, Zurich,  
1109 Switzerland. 244 pp.

1110 Yermolaeva, N.I., & Burmistrova, O.S. (2017). Zooplankton of the Lake Bolshoe  
1111 Shchuchye. Scientific Newsletter of Yamalo-Nenets Autonomous Region 1 (94), 15–20 (in  
1112 Russian).

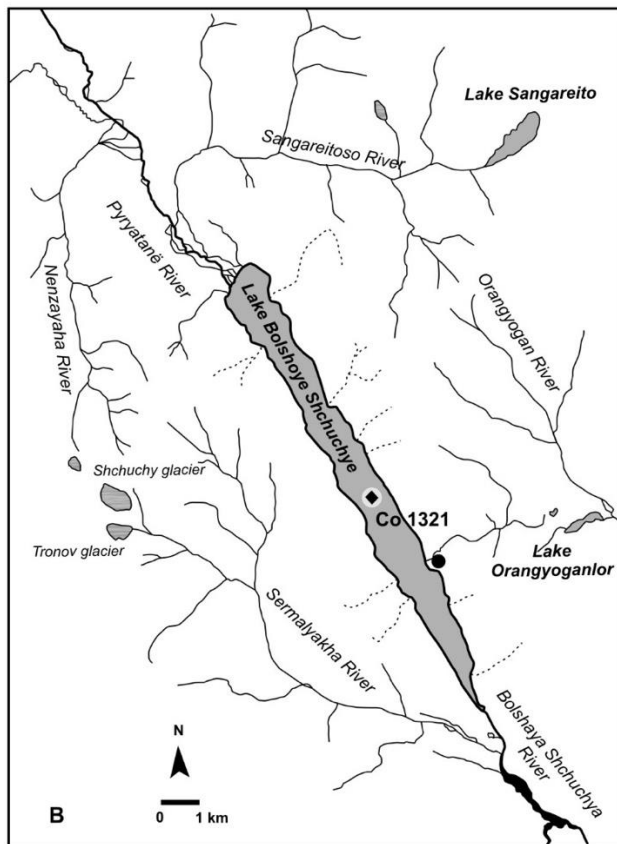
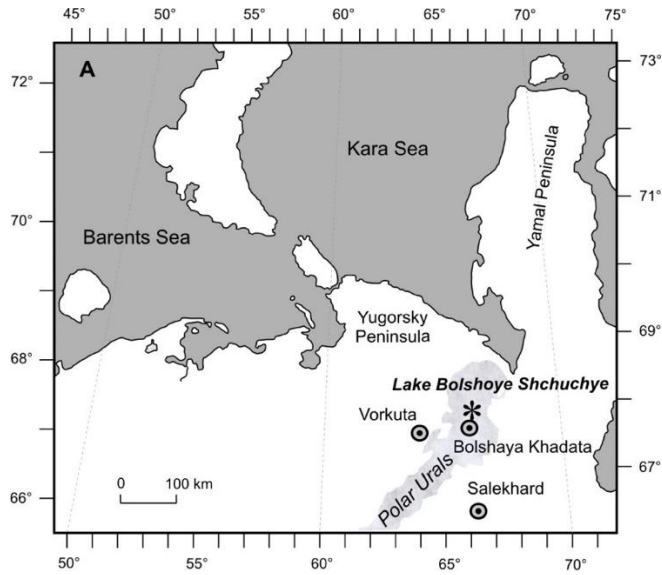
1113

1114 Table 1. Main geochemical characteristics of diatoms from Lake Bolshoye Shchuchye based on EDS data. Measured  $\delta^{18}\text{O}$  values ( $\delta^{18}\text{O}_{\text{meas}}$ ), calculated  
 1115 contamination ( $c_{\text{cont}}$ ; %) and  $\delta^{18}\text{O}$  values corrected for contamination ( $\delta^{18}\text{O}_{\text{corr}}$ ) are given.

| Core          | Sample depth (cm) | Age (cal. ka BP) | SiO <sub>2</sub> (%) | Al <sub>2</sub> O <sub>3</sub> (%) | Na <sub>2</sub> O (%) | MgO (%) | K <sub>2</sub> O (%) | CaO (%) | MnO (%) | FeO (%) | Total  | $\delta^{18}\text{O}_{\text{meas}}$ (‰) | $c_{\text{cont}}$ (%) | $\delta^{18}\text{O}_{\text{corr}}$ (‰) |
|---------------|-------------------|------------------|----------------------|------------------------------------|-----------------------|---------|----------------------|---------|---------|---------|--------|---|-----------------------|---|
| Co1321-3-SL   | surface           |                  | 98.77                | 0.52                               | 0.23                  | 0.14    | 0.03                 | 0.02    | 0.02    | 0.26    | 100.00 | 23.17                                   | 2.4                   | 23.44                                   |
| Co 1321-2     | 4.4               | 0.008            | 98.57                | 0.48                               | 0.55                  | 0.12    | 0.01                 | 0.05    | 0.05    | 0.17    | 100.00 | 23.41                                   | 2.2                   | 23.66                                   |
| Co 1321-2     | 20.9              | 0.327            | 98.02                | 0.71                               | 0.63                  | 0.20    | 0.01                 | 0.05    | 0.03    | 0.36    | 100.00 | 24.73                                   | 3.3                   | 25.15                                   |
| Co 1321-2     | 35.8              | 0.614            | 98.76                | 0.51                               | 0.37                  | 0.11    | 0.00                 | 0.02    | 0.03    | 0.22    | 100.00 | 25.06                                   | 2.4                   | 25.36                                   |
| Co 1321-2     | 54.1              | 0.956            | 97.44                | 0.86                               | 1.04                  | 0.15    | 0.03                 | 0.05    | 0.06    | 0.39    | 99.99  | 26.15                                   | 4.0                   | 26.71                                   |
| Co 1321-2     | 67.8              | 1.181            | 97.98                | 0.88                               | 0.46                  | 0.16    | 0.01                 | 0.07    | 0.01    | 0.43    | 100.00 | 24.51                                   | 4.1                   | 25.02                                   |
| Co 1321-31-II | 97.9              | 1.676            | 96.65                | 1.49                               | 0.86                  | 0.21    | 0.09                 | 0.08    | 0.02    | 0.61    | 100.00 | 23.61                                   | 7.2                   | 24.48                                   |
| Co 1321-31-II | 112.4             | 1.868            | 97.85                | 0.78                               | 0.69                  | 0.16    | 0.02                 | 0.04    | 0.06    | 0.40    | 100.00 | 29.22                                   | 3.6                   | 29.85                                   |
| Co 1321-32-I  | 152.7             | 2.378            | 98.21                | 0.53                               | 0.79                  | 0.14    | 0.00                 | 0.02    | 0.05    | 0.27    | 100.00 | 24.89                                   | 2.5                   | 25.20                                   |
| Co 1321-32-I  | 167.7             | 2.562            | 98.14                | 0.85                               | 0.38                  | 0.17    | 0.01                 | 0.06    | 0.02    | 0.39    | 100.00 | 28.06                                   | 3.9                   | 28.70                                   |
| Co 1321-32-I  | 187.5             | 2.804            | 98.01                | 0.75                               | 0.66                  | 0.15    | 0.02                 | 0.03    | 0.04    | 0.35    | 100.01 | 27.71                                   | 3.5                   | 28.26                                   |
| Co 1321-32-I  | 200.6             | 2.965            | 95.14                | 1.47                               | 2.58                  | 0.10    | 0.14                 | 0.13    | 0.03    | 0.41    | 100.00 | 24.47                                   | 6.8                   | 25.35                                   |
| Co 1321-32-I  | 215.4             | 3.178            | 97.89                | 0.81                               | 0.60                  | 0.18    | 0.01                 | 0.09    | 0.04    | 0.38    | 100.00 | 25.16                                   | 3.8                   | 25.65                                   |
| Co 1321-32-II | 235.2             | 3.462            | 97.58                | 1.09                               | 0.65                  | 0.13    | 0.07                 | 0.05    | 0.09    | 0.35    | 100.00 | 26.43                                   | 5.1                   | 27.17                                   |
| Co 1321-32-II | 249.8             | 3.672            | 98.04                | 0.74                               | 0.75                  | 0.10    | 0.01                 | 0.05    | 0.08    | 0.25    | 100.00 | 27.37                                   | 3.4                   | 27.89                                   |
| Co 1321-32-II | 265.8             | 3.904            | 98.09                | 0.85                               | 0.49                  | 0.16    | 0.01                 | 0.05    | 0.02    | 0.34    | 100.00 | 25.29                                   | 3.9                   | 25.81                                   |
| Co 1321-32-II | 281.8             | 4.136            | 97.50                | 0.97                               | 0.81                  | 0.15    | 0.04                 | 0.07    | 0.04    | 0.43    | 100.00 | 25.05                                   | 4.5                   | 25.64                                   |
| Co 1321-32-II | 298.1             | 4.372            | 97.73                | 0.65                               | 1.19                  | 0.03    | 0.03                 | 0.13    | 0.05    | 0.20    | 100.00 | 25.84                                   | 3.0                   | 26.25                                   |
| Co 1321-32-II | 314.5             | 4.611            | 96.01                | 1.89                               | 0.93                  | 0.30    | 0.18                 | 0.06    | 0.01    | 0.63    | 100.01 | 26.84                                   | 8.8                   | 28.22                                   |
| Co 1321-32-II | 330.3             | 4.842            | 97.89                | 0.89                               | 0.66                  | 0.09    | 0.02                 | 0.03    | 0.02    | 0.40    | 99.99  | 26.83                                   | 4.1                   | 27.45                                   |
| Co 1321-33-I  | 353.6             | 5.181            | 97.76                | 0.96                               | 0.74                  | 0.11    | 0.02                 | 0.04    | 0.03    | 0.34    | 99.99  | 26.31                                   | 4.5                   | 26.96                                   |
| Co 1321-33-I  | 368.6             | 5.392            | 96.58                | 1.53                               | 0.92                  | 0.21    | 0.09                 | 0.09    | 0.02    | 0.56    | 100.00 | 26.15                                   | 7.1                   | 27.19                                   |
| Co 1321-33-I  | 400.9             | 5.847            | 98.18                | 0.82                               | 0.45                  | 0.12    | 0.04                 | 0.11    | 0.04    | 0.24    | 100.00 | 25.62                                   | 3.8                   | 26.14                                   |
| Co 1321-33-I  | 425.6             | 6.227            | 96.45                | 1.87                               | 0.50                  | 0.34    | 0.14                 | 0.08    | 0.03    | 0.59    | 100.00 | 27.51                                   | 8.7                   | 28.94                                   |
| Co 1321-33-II | 434.8             | 6.369            | 96.83                | 1.26                               | 1.15                  | 0.17    | 0.06                 | 0.06    | 0.04    | 0.45    | 100.00 | 30.70                                   | 5.9                   | 31.83                                   |
| Co 1321-33-II | 450.8             | 6.613            | 97.16                | 1.25                               | 0.85                  | 0.14    | 0.02                 | 0.08    | 0.04    | 0.47    | 100.00 | 25.87                                   | 5.8                   | 26.69                                   |
| Co 1321-33-II | 465.9             | 6.821            | 97.98                | 1.00                               | 0.28                  | 0.14    | 0.06                 | 0.07    | 0.03    | 0.43    | 100.00 | 26.09                                   | 4.6                   | 26.75                                   |
| Co 1321-33-II | 483.1             | 7.057            | 98.12                | 0.89                               | 0.26                  | 0.15    | 0.05                 | 0.07    | 0.04    | 0.40    | 100.00 | 28.61                                   | 4.2                   | 29.31                                   |
| Co 1321-33-II | 499.1             | 7.277            | 96.04                | 1.69                               | 1.46                  | 0.08    | 0.15                 | 0.11    | 0.02    | 0.46    | 100.00 | 25.53                                   | 7.9                   | 26.64                                   |
| Co 1321-33-II | 534.5             | 7.628            | 97.09                | 1.35                               | 0.94                  | 0.13    | 0.04                 | 0.05    | 0.01    | 0.39    | 100.00 | 25.71                                   | 6.3                   | 26.60                                   |
| Co 1321-34-I  | 555.1             | 7.832            | 97.78                | 0.95                               | 0.49                  | 0.14    | 0.01                 | 0.08    | 0.04    | 0.51    | 100.00 | 27.44                                   | 4.4                   | 28.13                                   |
| Co 1321-34-I  | 572.6             | 8.008            | 97.76                | 0.82                               | 0.72                  | 0.06    | 0.01                 | 0.07    | 0.02    | 0.55    | 100.00 | 26.61                                   | 3.8                   | 27.17                                   |
| Co 1321-34-I  | 585.3             | 8.137            | 97.63                | 1.01                               | 0.77                  | 0.13    | 0.02                 | 0.07    | 0.03    | 0.36    | 100.00 | 28.14                                   | 4.7                   | 28.91                                   |
| Co 1321-34-I  | 602.8             | 8.316            | 97.31                | 0.99                               | 1.10                  | 0.03    | 0.03                 | 0.08    | 0.04    | 0.42    | 100.00 | 25.24                                   | 4.6                   | 25.85                                   |

|               |       |        |       |      |      |      |      |      |      |      |        |       |     |       |
|---------------|-------|--------|-------|------|------|------|------|------|------|------|--------|-------|-----|-------|
| Co 1321-34-I  | 617.6 | 8.477  | 97.16 | 1.12 | 0.81 | 0.15 | 0.09 | 0.18 | 0.05 | 0.45 | 100.00 | 25.74 | 5.2 | 26.46 |
| Co 1321-34-II | 667.6 | 9.012  | 97.96 | 1.09 | 0.37 | 0.14 | 0.03 | 0.14 | 0.01 | 0.26 | 100.00 | 25.77 | 5.1 | 26.48 |
| Co 1321-34-II | 684.7 | 9.191  | 96.05 | 1.93 | 1.01 | 0.30 | 0.12 | 0.08 | 0.07 | 0.41 | 99.95  | 26.58 | 9.0 | 27.97 |
| Co 1321-34-II | 698.6 | 9.336  | 97.49 | 1.32 | 0.36 | 0.17 | 0.11 | 0.10 | 0.04 | 0.42 | 100.00 | 26.95 | 6.1 | 27.90 |
| Co 1321-34-II | 713.1 | 9.483  | 96.50 | 0.92 | 2.15 | 0.07 | 0.02 | 0.12 | 0.00 | 0.23 | 100.00 | 26.36 | 4.3 | 26.98 |
| Co 1321-35-I  | 768.9 | 10.050 | 97.26 | 1.62 | 0.29 | 0.21 | 0.14 | 0.14 | 0.03 | 0.32 | 100.00 | 26.24 | 7.5 | 27.36 |
| Co 1321-35-I  | 778.4 | 10.146 | 98.24 | 1.05 | 0.13 | 0.12 | 0.03 | 0.14 | 0.00 | 0.30 | 100.00 | 25.92 | 4.9 | 26.61 |
| Co 1321-35-I  | 787.4 | 10.237 | 96.13 | 1.97 | 0.62 | 0.35 | 0.14 | 0.15 | 0.05 | 0.59 | 100.00 | 25.49 | 9.2 | 26.81 |
| Co 1321-35-I  | 802.3 | 10.389 | 95.51 | 1.74 | 2.08 | 0.09 | 0.18 | 0.08 | 0.04 | 0.29 | 100.00 | 25.16 | 8.1 | 26.28 |
| Co 1321-35-I  | 817.0 | 10.538 | 96.46 | 1.83 | 0.50 | 0.29 | 0.17 | 0.20 | 0.02 | 0.53 | 100.00 | 26.78 | 8.5 | 28.12 |
| Co 1321-35-I  | 835.3 | 10.724 | 96.68 | 1.77 | 0.74 | 0.22 | 0.07 | 0.07 | 0.03 | 0.42 | 100.00 | 26.49 | 8.3 | 27.75 |
| Co 1321-35-II | 851.3 | 10.887 | 96.01 | 2.00 | 0.65 | 0.37 | 0.16 | 0.18 | 0.05 | 0.56 | 100.00 | 25.30 | 9.3 | 26.62 |
| Co 1321-35-II | 872.4 | 11.110 | 96.21 | 2.02 | 0.55 | 0.27 | 0.17 | 0.23 | 0.06 | 0.50 | 100.00 | 25.86 | 9.4 | 27.25 |
| Co 1321-35-II | 915.2 | 11.555 | 94.76 | 1.99 | 2.20 | 0.21 | 0.12 | 0.17 | 0.07 | 0.48 | 100.00 | 26.43 | 9.3 | 27.86 |

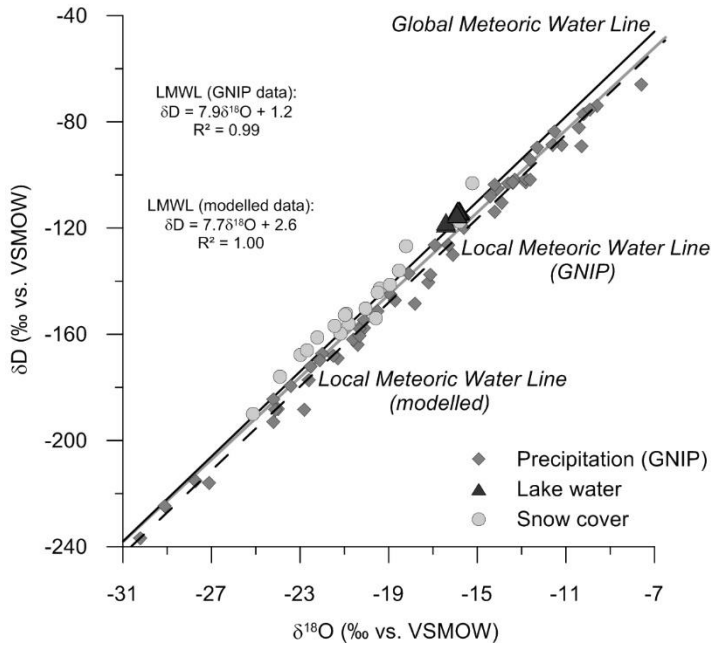
1117 **Figure 1.** A. Schematic maps of the Polar Urals including the study site and other points of  
1118 interest modified from Andreev et al. (2005). B. Location of Lake Bolshoye Shchuchye  
1119 ( $67^{\circ}53'N$ ;  $66^{\circ}19' E$ ; 186 m a.s.l.) with the position of the Co 1321 sediment core (black diamond)  
1120 and the water sampling site (grey circle); as well as location of the snow cover column (black  
1121 circle). The sketch was adapted from Regnéll et al. (2019). The Shchuchy and Tronov glaciers  
1122 are outside the Lake Bolshoye Shchuchye catchment.



1123

1124

1125 **Figure 2.**  $\delta^{18}\text{O}$ – $\delta\text{D}$  diagram for water samples from Lake Bolshoye Shchuchye and snow  
1126 cover. Additionally, GNIP data for regional precipitation, the Global Meteoric Water Line  
1127 (GMWL;  $\delta\text{D} = 8 \cdot \delta^{18}\text{O} + 10$ ; Craig 1961; Rozanski et al., 1993) and Local Meteoric Water Line  
1128 (LMWL) based on GNIP data (black dash line; IAEA/WMO, 2021) and LMWL modelled from  
1129 OIPC (grey solid line; Bowen, 2021) are given.  
1130

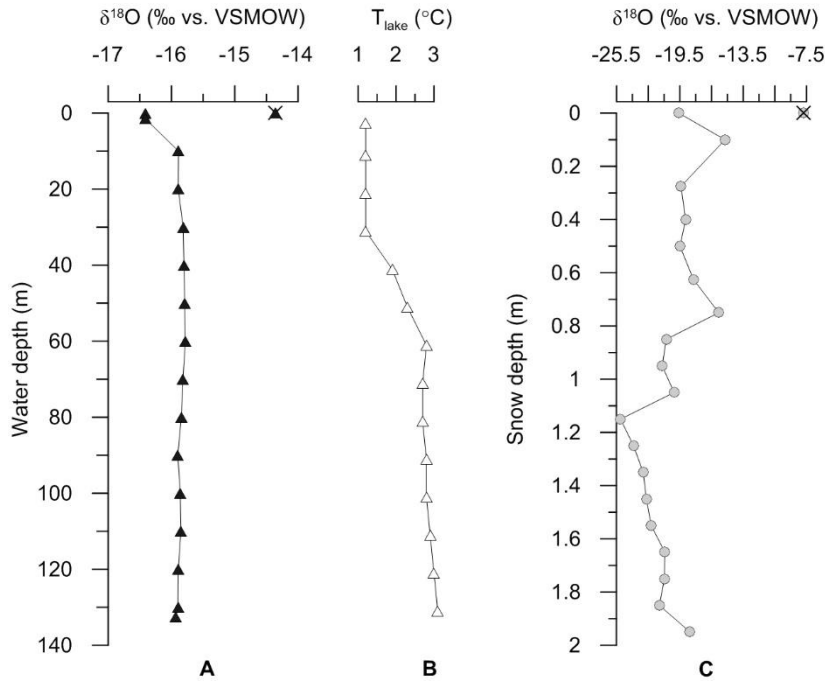


1131

1132

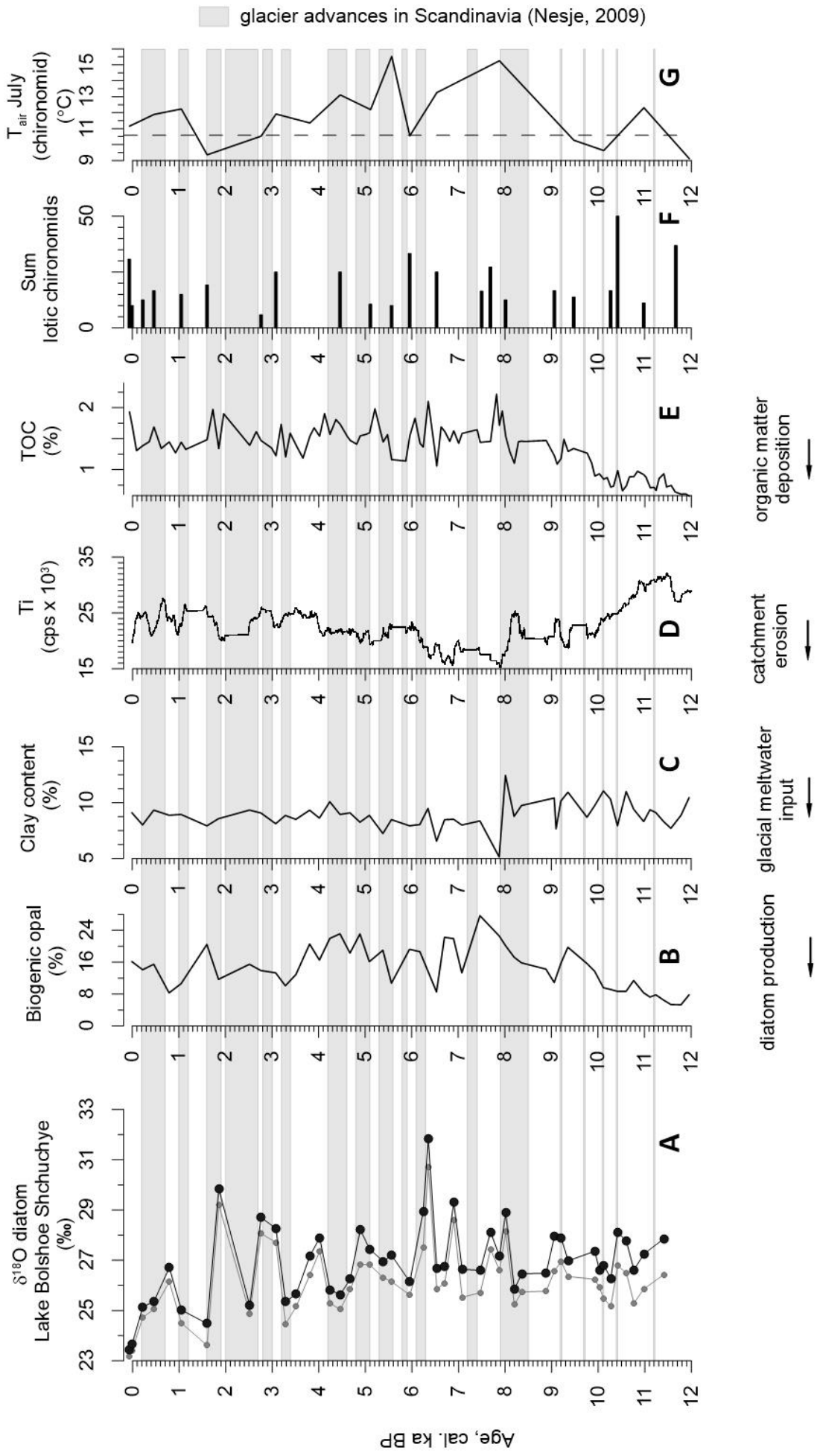
1133

1134 **Figure 3.** Depth profiles. A. Oxygen isotope composition of water from Lake Bolshoye  
 1135 Shchuchye. B. Lake water temperature, measured 50 m north of the coring site. C. Oxygen  
 1136 isotope composition of snow cover. Water and snow samples excluded from interpretation are  
 1137 marked as crossed out signs.  
 1138

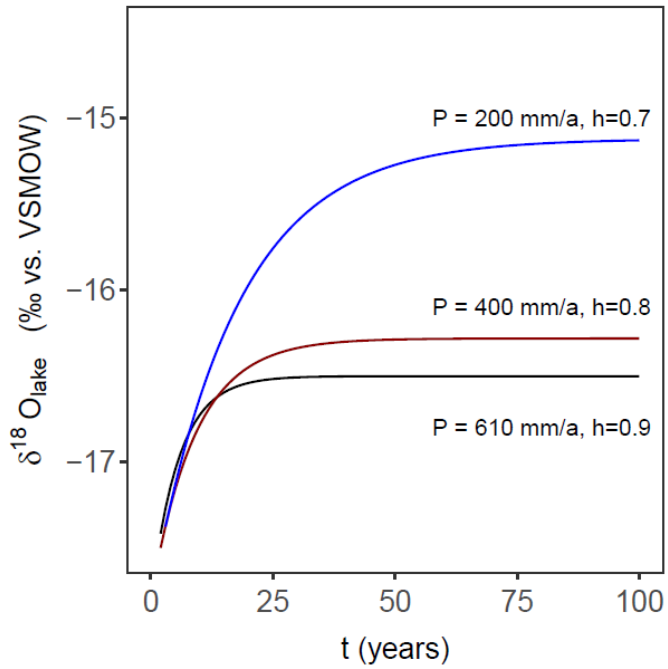


1139  
 1140

1141 **Figure 4.** (A) Holocene oxygen isotope composition of diatoms from Lake Bolshoye  
 1142 Shchuchye (grey raw data:  $\delta^{18}\text{O}_{\text{meas}}$ ; black: contamination-corrected  $\delta^{18}\text{O}_{\text{corr}}$  values, referred to as  
 1143  $\delta^{18}\text{O}_{\text{diatom}}$ ) compared to other lake internal parameters, such as: (B) the biogenic silica  
 1144 percentage, as proxy for the diatom production, (C) clay content, as glacial meltwater proxy, (D)  
 1145 Ti cps (counts per second), a proxy for detrital input and catchment erosion. (E) TOC content, as  
 1146 proxy for organic matter input to the lake, as well as (F) the sum of lotic chironomids, indicative  
 1147 for riverine influx, and (G) a chironomid-based July air temperature reconstruction for Lake  
 1148 Bolshoye Shchuchye. The dashed line corresponds to the modern mean July air temperature (of  
 1149  $10.6^\circ\text{C}$ ). All lake internal proxies are introduced and discussed in detail in Lenz et al. (2021).  
 1150 Greyscales indicate periods of known glacier advances in Scandinavia (Nesje, 2009).



1152 **Figure 5.** Modelled evaporative enrichment of lake water over time for three different  
1153 scenarios of precipitation and atmospheric humidity. The black line represents present-day  
1154 precipitation (P) and humidity (h) level, whereas the blue and red lines characterize hypothetical  
1155 conditions with much lower precipitation and humidity.



1156

1157

1158 **Figure 6.** Geomorphological and snow characteristics of the Lake Bolshoye Shchuchye  
 1159 catchment. (A) Digital Elevation Model (DEM), (B) Slope (in degrees), (C) snow depth (in cm)  
 1160 and (D) Snow water equivalent (SWE, in mm) .

1161

1162

1163

1164

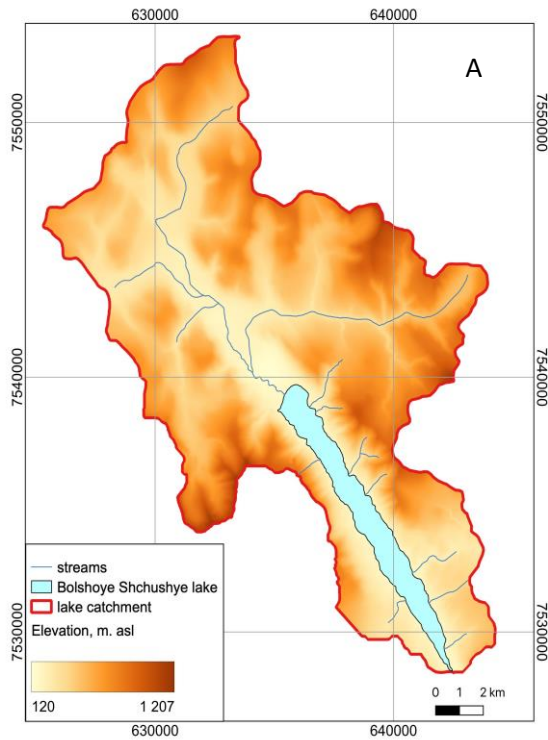
1165

1166

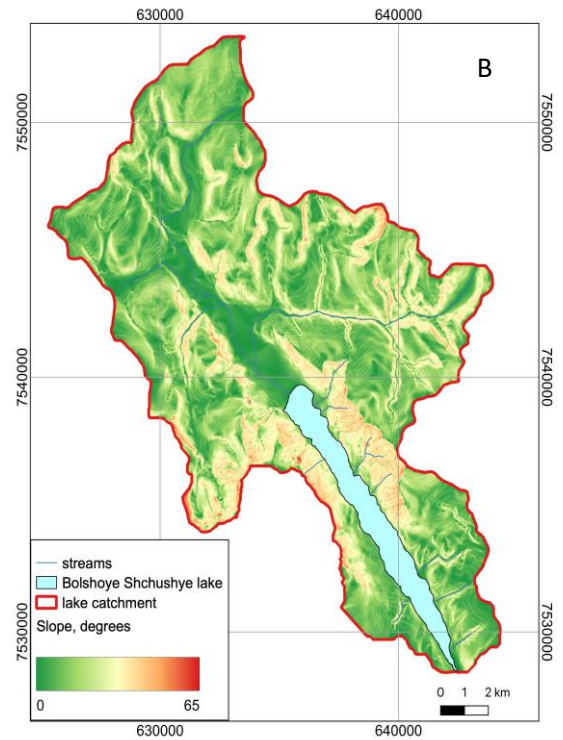
1167

1168

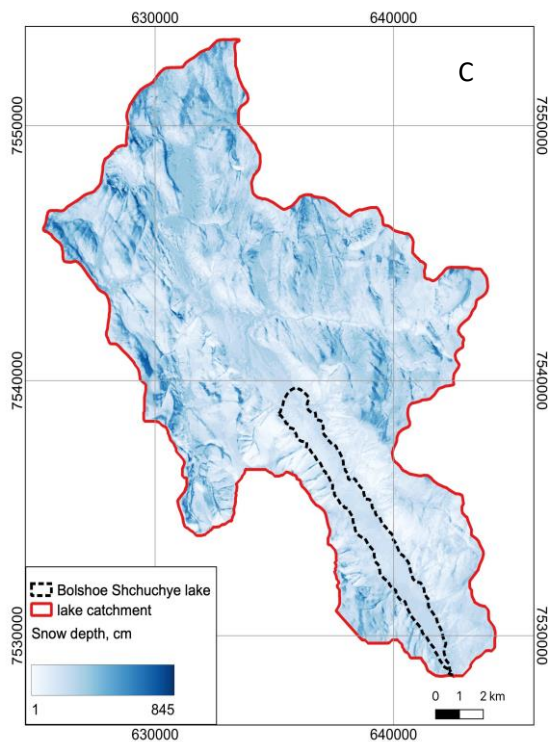
1169



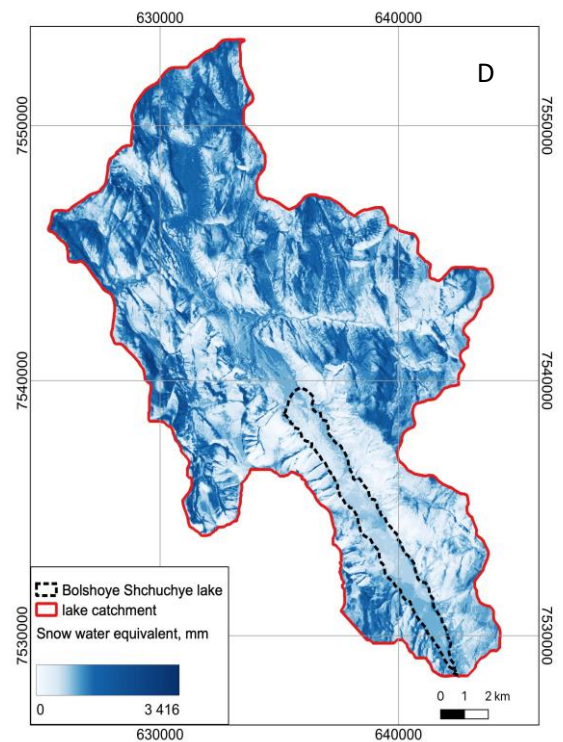
**Digital Elevation Model**



**Slope**

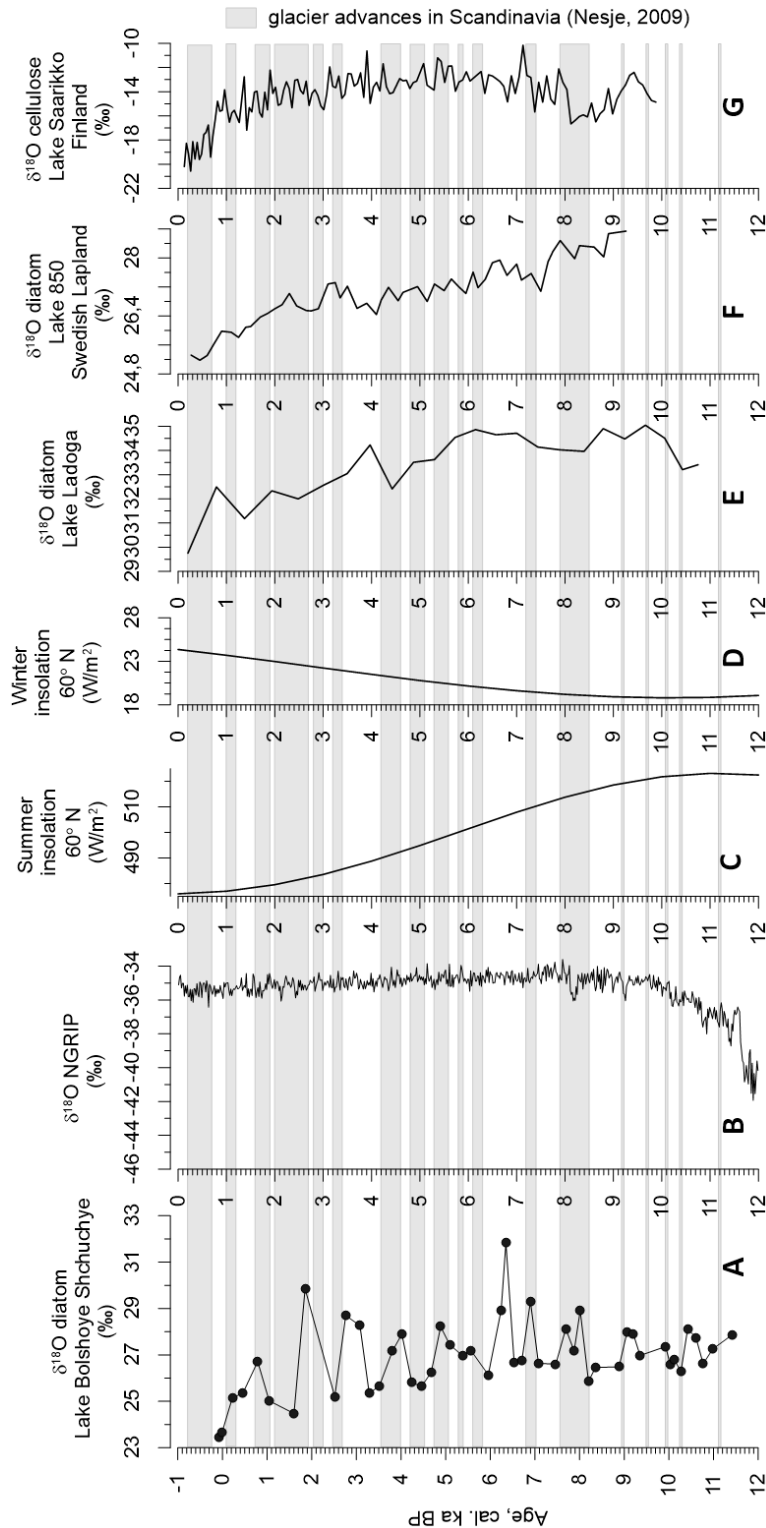


**Snow Depth**

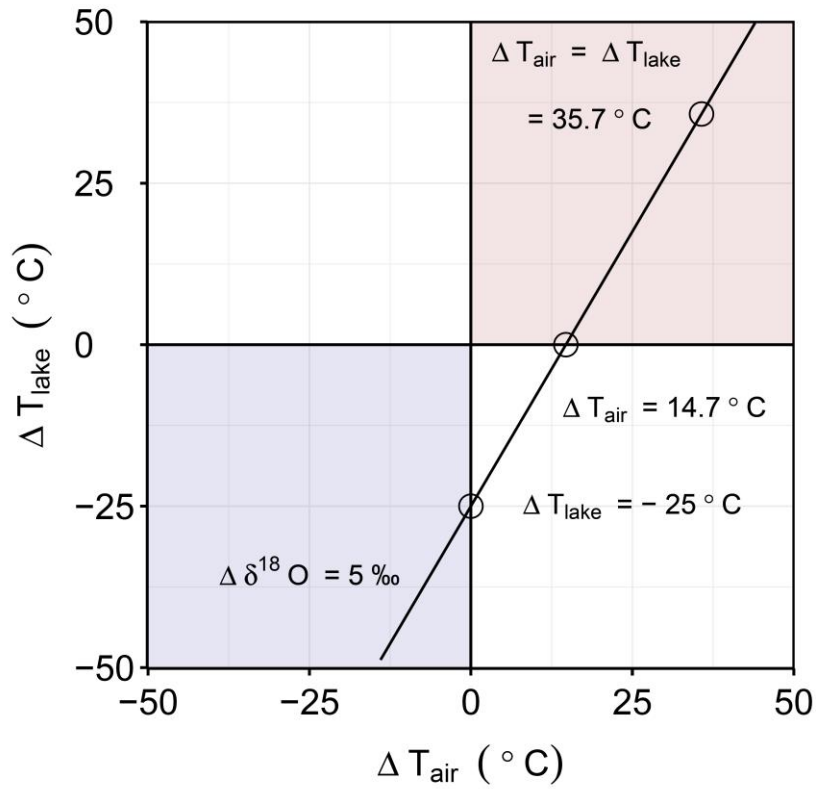


**Snow Water Equivalent**

1170 **Figure 7.** (A) Oxygen isotope composition of diatoms from Lake Bolshoye Shchuchye  
 1171 compared to other North Hemispheric (NH) climate reconstructions, such as (B) the NGRIP  
 1172 oxygen isotope record from Greenland ice (Svensson et al., 2008), an proxy for the NH air  
 1173 temperature, (C and D) the NH summer and winter insolation at 60° N (Berger & Loutre, 1991),  
 1174 as well as other regional diatom-based oxygen isotope records (E) from Lake Ladoga (Kostrova  
 1175 et al., 2019) and (F) Lake 850, Swedish Lapland (Shemesh et al., 2001), and (G) a cellulose-  
 1176 based reconstruction from Lake Saarikko, Finland (Heikkilä et al., 2010).



1178 **Figure S1.** Scenario functions of  $T_{\text{air}}$  and  $T_{\text{lake}}$  changes corresponding to a 5‰-shift in  
 1179  $\delta^{18}\text{O}_{\text{diatom}}$ , based on a diatom-temperature coefficient of  $-0.2\text{‰}/^{\circ}\text{C}$  (Swann & Leng, 2009; Dodd  
 1180 & Sharp, 2010) and the regional temperature relation between monthly mean  $\delta^{18}\text{O}_{\text{prec}}$  and  $T_{\text{air}}$  of  
 1181  $\delta^{18}\text{O}_{\text{prec}} = +0.34\text{‰}/^{\circ}\text{C}$  (Salekhard; IAEA/WMO, 2021).



1182